

AD-A124 796

EVALUATION OF A DETECTION SYSTEM EMPLOYING TWO SILICON
SEMICONDUCTORS FOR. (U) AIR FORCE INST OF TECH
WRIGHT-PATTERSON AFB OH SCHOOL OF ENGI. M L ANDREWS
MAR 82 AFIT/GNE/PH/82M-1 F/G 18/2

1/1

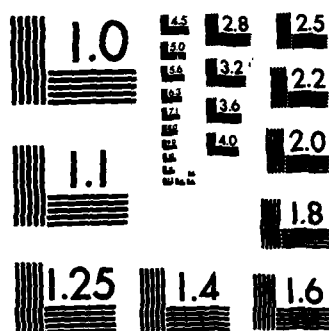
UNCLASSIFIED

NL

END

FILMED

DTIC



AD A124796

EVALUATION OF A DETECTION SYSTEM
EMPLOYING TWO SILICON SEMICONDUCTORS
FOR THE ANALYSIS OF RADIOACTIVE
NOBLE GASES

THESIS

Wayne L. Andrews, Jr.
AFIT/GNE/PH/82M-1 Capt USAF

DTIC FILE COPY

DTIC
ELECTE
FEB 23 1983
S D E

Approved for public release; distribution unlimited.

88 02 02 09

EVALUATION OF A DETECTION SYSTEM EMPLOYING
TWO SILICON SEMICONDUCTORS FOR THE
ANALYSIS OF RADIOACTIVE NOBLE GASES

THESIS

Presented to the Faculty of the School of Engineering
of the Air Force Institute of Technology

Air University

in Partial Fulfillment of the
Requirements for the Degree of
Master of Science

Accession For	
NTIS GRA&I	<input checked="checked" type="checkbox"/>
DTIC TAB	<input type="checkbox"/>
Unannounced	<input type="checkbox"/>
Justification	
By	
Distribution/	
Availability Codes	
Dist	Avail and/or Special
A	

Wayne L. Andrews, Jr., B.S., M.B.A.

Capt

USAF

Graduate Nuclear Engineering

March 1982



Approved for public release; distribution unlimited.

Preface

The purpose of this study was to identify and evaluate the various characteristics of a radiation detection system and to examine its potential for the detection of ^{131m}Xe in the presence of ^{133}Xe . Although many equipment problems were encountered during this project, I was able to collect enough data to perform the necessary evaluation of the system's characteristics and to develop a procedure for the detection and measurement of ^{131m}Xe in the presence of ^{133}Xe .

I am indebted to Dr. George John, my thesis advisor, for his patience, guidance and criticisms which were helpful throughout this study. I am also grateful to Mr. Hendricks whose assistance in the laboratory was invaluable. Finally, I wish to acknowledge my gratitude to my wife Donna, for her patience and encouragement and to Jill Marie and Wayne Linwood who will one day soon have a full-time father once again.

Contents

	<u>Page</u>
Preface	ii
List of Figures	v
List of Tables	vii
Abstract	viii
I. Introduction	1
Purpose	1
Background	1
Development	5
II. Characteristics of the Noble Gas Sample	6
Introduction	6
Production	6
Nuclear Decay Data	8
III. Equipment	13
General Description and Procedure	13
Cryostat	15
Gas-handling and Measuring Equipment	18
Detectors and Their Characteristics	20
Electronics for Pulse Processing and Analysis	22
IV. Time To Amplitude Converter and Coincidence Counting	24
Purpose	24
Time To Amplitude Converter (TAC)	24
Chance Coincidences	25
Time Spectrum	26
Measurement of Source Activity and Detector Efficiencies	27
Experimental Applications	28
V. Factors Affecting Detection	29
Introduction	29
Migration	29
Self-Absorption	30
Carrier Gas Fluorescence	31
Geometry	32
Detector Efficiencies	33
Resolution	34

Contents

	<u>Page</u>
VI. Data Analysis and Results	36
Introduction	36
Migration	36
Self-Absorption	38
Carrier Gas Fluorescence	42
Background Radiation	43
Time Spectroscopy	44
Xenon-131m Energy Spectra	45
Xenon-133 Energy Spectra	48
Combined Spectra	50
VII. Conclusions and Recommendations	52
Bibliography	54
Appendix: Xenon-133 X-ray Energy Spectra Showing the Effects of Carrier Gas Fluorescence . .	56
Vita	62

List of Figures

<u>Figure</u>		<u>Page</u>
1	Xenon-131m Decay Scheme	10
2	Xenon-133 Decay Scheme	10
3	Total System Components and General Configuration	13
4	Cross-sectional View of Detection System Assembly	14
5	Detectors and Sample Chamber	15
6	Gas-handling System	19
7	Block Diagram of Electronic Equipment	23
8	Multichannel Analyzer Time Spectrum	27
9	Count Rate Decrease After the Admission of Sample to Chamber	36
10	Time for Sample to Reach Its Characteristic Decay vs. Heater Current Applied	38
11	Self-Absorption of Xenon-131m Internal Conversion Electrons	39
12	Xenon-133 Carrier Gas X-ray Fluorescence	42
13	Xenon-131m Time Spectrum	44
14	Xenon-131m Electron Energy Spectrum	46
15	Xenon-131m X-ray Energy Spectrum	47
16	Xenon-133 Electron Energy Spectrum	48
17	Xenon-133 X-ray Energy Spectrum	49
18	Combined X-ray Energy Spectrum of Both Xenon-131m and Xenon-133	50
19	Xenon-133 X-ray Energy Spectrum - Sample Thickness = 0.02766 cm	57
20	Xenon-133 X-ray Energy Spectrum - Sample Thickness = 0.03319 cm	58

List of Figures

<u>Figure</u>		<u>Page</u>
21	Xenon-133 X-ray Energy Spectrum - Sample Thickness = 0.03872 cm	59
22	Xenon-133 X-ray Energy Spectrum - Sample Thickness = 0.04426 cm	60
23	Xenon-133 X-ray Energy Spectrum - Sample Thickness = 0.04979 cm	61

List of Tables

<u>Table</u>	<u>Page</u>
I. Cumulative Fission Yields for Xenon	7
II. The Effect of Decay Time on the Relative Activity of Radioactive Noble Gas Mixtures from ^{235}U Fission	8
III. Characteristic Radiations of $^{131\text{m}}\text{Xe}$ and ^{133}Xe . . .	9
IV. Physical Properties of Xenon	11
V. Detector Intrinsic Photopeak Efficiencies	33
VI. Detector Resolutions	35
VII. $^{131\text{m}}\text{Xe}$ Self-Absorption Factors	40

Abstract

This report presents a study of the characteristics of a radiation detection system for the analysis of radioactive noble gases. The sample gas is condensed in a chamber between two planar lithium-drifted silicon semiconductor detectors. The analysis was limited to two radioisotopes of xenon, ^{131m}Xe and ^{133}Xe , which are produced in nuclear fission. X-ray spectroscopy was used in an attempt to quantify ^{131m}Xe in the presence of ^{133}Xe . In previous research using this system, the sample gas deposited itself in the sample chamber in an uneven and unpredictable manner. Modifications were made to the sample chamber and the gas now deposits itself predictably and reproducibly. Also, the effects of self-absorption and carrier gas x-ray fluorescence were analyzed and quantified. Finally, it was found that the system could quantify ^{131m}Xe in the presence of ^{133}Xe using a simple three step procedure. Recommendations were made for further study with this system.

EVALUATION OF A DETECTION SYSTEM EMPLOYING TWO SILICON SEMICONDUCTORS FOR THE ANALYSIS OF RADIOACTIVE NOBLE GASES

I. Introduction

Purpose

Radioactive noble gases are produced in significant quantities by nuclear reactors and spent-fuel reprocessing plants. The release of these radioactive gaseous effluents constitute a potentially significant impact on the health and safety of the general populace. Therefore, it is imperative that a detection technique is developed which can accurately determine which noble gas radioisotopes are being emitted and in what quantities. This report presents a study of the characteristics of a radiation detection system for analyzing radioactive noble gases. The sample gas is condensed in a chamber between two planar lithium-drifted silicon (Si(Li)) semiconductor detectors. The analysis was limited to two radioisotopes of xenon, ^{133}Xe and $^{131\text{m}}\text{Xe}$, which are produced in nuclear fission. Coincidence techniques were used in an attempt to detect and quantify a relatively small amount of $^{131\text{m}}\text{Xe}$ in the presence of a much larger amount of ^{133}Xe .

Background

Hunt (Ref 8) used the same detection system as currently under evaluation in his analysis of $^{131\text{m}}\text{Xe}$ and ^{133}Xe . His

experimental analysis was hampered by three problems. The first was a significant amount of x-ray fluorescence from the carrier gas which he felt he could not quantify. Secondly, he observed excessive degradation in electron energy as a result of self-absorption. Finally, he hypothesized that the sample gas was migrating to unfavorable areas of the sample chamber thus decreasing the geometry factor, increasing self-absorption and backscatter of electrons and affecting the reproducibility of the procedure. Modifications were made to Hunt's detection system with the intent of either eliminating or at least minimizing the above mentioned problems. Chapter V describes these problems more fully and explains the modifications which were made to the system.

Horrocks and Studier were the first to demonstrate that it was possible to measure radioactive noble gases in liquid scintillator systems (Ref 7). Since that time, liquid scintillation spectroscopy has been the only technique which has been successful in detecting and measuring ^{131m}Xe in the presence of ^{133}Xe . The principal benefits of using liquid scintillation are 1) a geometry factor and intrinsic efficiency for electrons of nearly 100% since the radioisotopes are dissolved in the liquid scintillator, and 2) reduction of energy degradation from self-absorption and scattering of electrons. On the other hand, liquid scintillators have a very low intrinsic efficiency for electromagnetic radiation and an inherently poor spectral resolution.

The principal reasons for investigating the use of semiconductor detectors for the analysis of radioactive noble gases lies in their superior resolution as well as a greater intrinsic efficiency for electromagnetic radiation than does a liquid scintillator detector. For example, for the xenon characteristic x rays of about 30 keV, the liquid scintillator has a photoelectric mass absorption coefficient of only $0.05 \text{ cm}^2/\text{gm}$ whereas for silicon the value is $1.17 \text{ cm}^2/\text{gm}$ (Ref 19). Thus the intrinsic efficiency of a silicon semiconductor of a given thickness can be over twenty times that of a liquid scintillator of the same thickness for the characteristic x rays of xenon. The limiting value for energy resolution of a detector when measured in terms of the full width at half maximum (FWHM) of the full energy peak is proportional to the square root of the energy required to create one electron hole pair (ϵ) times the Fano factor for that particular detector (Ref 10:481). For scintillators this quantity is approximately 14 (Ref 17:66) whereas for semiconductors it is 0.6 (Ref 10:363). Thus, one can immediately see that detector resolution can be approximately twenty-three times smaller for semiconductors than for liquid scintillators.

In addition, certain researchers have recently expressed some interest in the use of room temperature semiconductors for detecting ^{131}mXe in the presence of ^{133}Xe . Although the system in this study is maintained at liquid nitrogen temperatures, many of its characteristics will be similar, if not identical to those of a room temperature semiconductor detec-

tion system. Thus the results of this study may be used for determining the feasibility of a room temperature semiconductor detection system (Ref 9).

The four methods of radiation analysis which could possibly be used to quantify ^{131m}Xe in the presence of ^{133}Xe are 1) x-ray spectroscopy, 2) gamma ray spectroscopy, 3) internal conversion electron analysis and, 4) coincidence analysis techniques. X-ray spectroscopy is possible if the spectral resolution of the detection system is at least 0.5 keV or better to differentiate between the xenon characteristic x rays emitted in the decay of ^{131m}Xe (K_{α_1} is at 29.78 keV) and the cesium characteristic x rays emitted in the decay of ^{133}Xe (K_{α_1} is at 30.97 keV). In addition, xenon x-ray fluorescence needs to be quantified before an accurate analysis of the relative amounts of each radioisotope from the intensity of the characteristic x rays of xenon can be performed. Xenon-131m has a very high internal conversion coefficient ($e_K:\gamma = 32:1$) and emits a gamma ray in only 2% of its decays. Thus gamma ray spectroscopy is not attempted in this study. Although internal conversion electron analysis appears promising due to ^{131m}Xe 's high internal conversion coefficient, this analysis is complicated by the beta spectrum associated with ^{133}Xe . Xenon-133's principal decay mode is β -emission, with a maximum beta energy of 364.3 keV. In addition, the effects of self-absorption on the internal conversion electrons of ^{131m}Xe must be quantified. Finally, coincidence analysis techniques

can be used to reduce the background effects (in this case the beta spectrum of ^{133}Xe) and thus enhance the internal conversion electron spectral peaks. In this study the use of x-ray, electron, and x-ray-electron coincidence spectroscopy was examined to accomplish the goal of detecting and measuring $^{131\text{m}}\text{Xe}$ in the presence of ^{133}Xe .

Development

Information concerning the noble gas of interest, xenon, is presented in Chapter II. In Chapter III a brief description of the equipment and its set-up is given. Chapter IV describes time spectroscopy and how coincidence techniques were applied to this study. Some of the factors which affect detection are discussed in Chapter V. Chapter VI describes the data analysis and results of the study and the conclusions and recommendations are presented in Chapter VII.

II. Characteristics of the Noble Gas Sample

Introduction

Xenon, chemical element number 54 and the fifth member of the family of inert gases, is a colorless, odorless, and tasteless gas. Natural xenon has an atomic weight of 131.30 and consists of nine stable isotopes whose mass numbers range from 124 through 136 (Ref 3:1106). In addition, 27 radioactive isotopes and isomers have been produced artificially in nuclear reactors and in particle accelerators (Ref 20:29). Although xenon is continuously being formed in the earth's crust by spontaneous or neutron induced fission, the rate of formation is so slow as to be insignificant. Thus, the xenon content of dry air of 0.086 parts per million by volume may be considered constant (Ref 4:3). It is, in fact, the rarest of all of the stable elements with an estimated abundance of only $2.9 \times 10^{-9}\%$ of the earth's crust (Ref 5:796).

Production

Xenon and krypton are the principal noble gases produced by nuclear fission. The gaseous effluents of operating nuclear reactors and spent-fuel reprocessing plants contain significant quantities of both stable and radioactive isotopes of these two noble gases. Table I lists the cumulative fission yields for the principal isotopes of xenon from the fissioning of ^{235}U .

Table I
Cumulative Fission Yields for Xenon

Isotope	Half-life	Fission Yield (%)
^{131m}Xe	12.0 days	0.017
^{131}Xe	Stable	2.770
^{132}Xe	Stable	4.130
^{133m}Xe	2.26 days	0.190
^{133}Xe	5.27 days	6.770
^{134}Xe	Stable	7.190
^{135m}Xe	15.7 minutes	1.050
^{135}Xe	9.20 hours	6.720
^{136}Xe	Stable	6.120
^{137}Xe	3.80 minutes	5.940
^{138}Xe	14.2 minutes	6.240
^{139}Xe	40.0 seconds	4.960

(Ref 14:69)

At first glance, the very low value for the fission yield of ^{131m}Xe would seem to indicate that this particular radioisotope does not make a significant contribution to the total activity produced by radioactive noble gas effluents. At early times, this is quite true, but as Table II shows, ^{131m}Xe because of its longer half-life, contributes increasingly to the total activity of the noble gases as the others decay away. Only ^{131m}Xe , ^{133}Xe , and ^{133m}Xe have half-lives reasonably long enough to be considered in this study. From the data in Table I one can compute that after only 9.7

Table II

The Effect of Decay Time on the Relative Activity
of Radioactive Noble Gas Mixtures from ^{235}U Fission*.

Isotope	Half-Life	Percent of Total Activity After Indicated Decay Time			
		2 min	2 hrs	3 days	60 days
^{139}Xe	41.0 sec	3.0			
^{89}Kr	3.2 min	8.2			
^{137}Xe	3.8 min	11.3			
$^{135\text{m}}\text{Xe}$	15.0 min	4.6	0.1		
^{138}Xe	17.0 min	14.1	0.3		
^{87}Kr	1.3 hrs	7.3	5.7		
$^{83\text{m}}\text{Kr}$	1.9 hrs	1.3	1.4		
^{88}Kr	2.8 hrs	10.2	13.5		
$^{85\text{m}}\text{Kr}$	4.4 hrs	4.2	6.7		
^{135}Xe	9.2 hrs	17.2	32.2	0.5	
$^{133\text{m}}\text{Xe}$	2.3 days	0.5	1.0	1.5	
^{133}Xe	5.3 days	18.0	30.0	96.7	2.5
$^{131\text{m}}\text{Xe}$	12.0 days	0.1	0.2	0.8	1.0
^{85}Kr	10.7 yrs	0.1	0.1	0.5	96.5

(Ref 2:76) *thermal neutrons

days the concentration of $^{131\text{m}}\text{Xe}$ is greater than that of $^{133\text{m}}\text{Xe}$. Thus, it was decided to use the radioisotopes $^{131\text{m}}\text{Xe}$ and ^{133}Xe in this study.

Nuclear Decay Data

The decay schemes and amounts of radiation emitted by $^{131\text{m}}\text{Xe}$ and ^{133}Xe are presented in Figures 1 and 2 and in Table III.

Table III
Characteristic Radiations of ^{131m}Xe and ^{133}Xe

Radiation Type	Energy (keV)	Fraction per Decay
<u>^{131m}Xe</u>		
Auger-L	3.43	0.75
Auger-K	24.6	0.068
ce-K	129.369	0.612
ce-L	158.477	0.286
ce-M	162.788	0.0650
ce-NOP	163.722	0.0178
X ray L	4.1	0.08
X ray K	29.4580	0.155
X ray K $_{\alpha_2}$	29.7790	0.287
X ray K $_{\alpha_1}$	33.6	0.102
X ray K $_{\beta}$	163.722	0.0178
<u>^{133}Xe</u>		
Auger-L	3.55	0.497
Auger-K	25.5	0.056
ce-K	45.012	0.533
ce-L	75.283	0.081
ce-M	79.780	0.016
ce-NOP	80.766	0.004
β^- maximum	346.3	0.993
average	100.6	
X ray L	4.29	0.061
X ray K	30.625	0.136
X ray K $_{\alpha_2}$	30.973	0.253
X ray K $_{\alpha_1}$	35.0	0.091
X ray K $_{\beta}$	80.997	0.365

(Ref 11:138)

Xenon-131m is an isomeric state of stable ^{131}Xe and is the radioactive progeny of Iodine-131. Xenon-131m has a high internal conversion coefficient ($e_K:\gamma = 32:1$) and thus, its energy spectrum is dominated by internal conversion electrons, characteristic xenon K-shell x rays and Auger electrons.

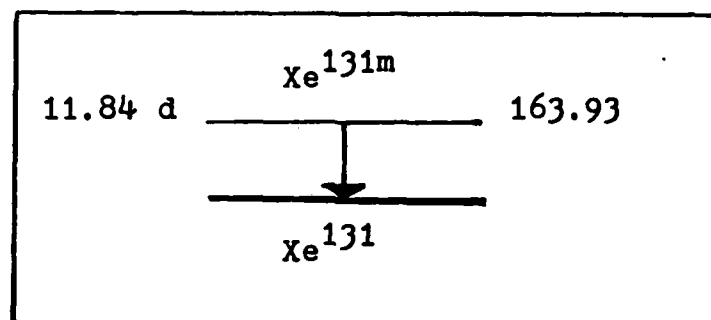


Figure 1. Xenon-131m Decay Scheme
(Ref 12:659)

Xenon-133 is a beta emitter which decays primarily (99.3%) to the first excited state (81 keV) of ^{133}Cs . This state has a moderate internal conversion coefficient ($e_K:\gamma = 1.4:1$). Xenon-133's energy spectrum is dominated by the beta decay spectrum with a maximum beta particle energy of

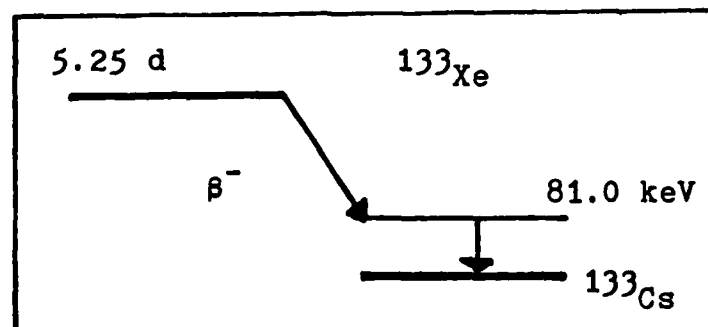


Figure 2. Xenon-133 Decay Scheme
(Ref 12:660)

Table IV
Physical Properties of Xenon

<u>Solid State</u>			
Triple point	Temperature	K	161.36
	Pressure	Torr	611
	Density (solid)	g/cc	3.540
	Density (liquid)	g/cc	3.076
Heat of Fusion		cal/mole	548.5
Vapor Pressure @ LN ₂		Torr	0.00137
<u>Liquid State</u>			
Normal boiling point		C	-108.12
Heat of vaporization at b.p.		cal/mole	3020.0
Density at b.p.		g/cc	2.987
Calorimetric entropy at b.p.		cal/mole/deg	37.66
Statistical entropy at b.p.		cal/mole/deg	37.58
Critical Temperature		C	16.59
Critical Pressure		atm	57.64
Critical Density		g/cc	1.100
<u>Gaseous State</u>			
Density at STP		g/l	5.8971
Specific heat at 25°C at 1 atm		cal/mole	4.968
Thermal conductivity @ 0°C, 1 atm		cal/cm/sec	0.0000123
Refractive index @ 0°C, 5893 Å			1.000702
Dielectric constant @ 25°C, 1 atm			1.001238
Viscosity @ 1 atm, 20°C		micropoise	227.40

(Ref 5:799)

346 keV and an average energy of 100.6 keV. Superimposed on the beta decay spectrum will be two internal conversion peaks at 45 keV and 79 keV, the gamma peak at 81 keV, cesium characteristic x rays at 31 keV and 35 keV and, finally, xenon characteristic x rays due to fluorescence of the carrier gas at 29 keV and 33 keV.

III. Equipment

General Description and Procedure

The system used for handling and analyzing radioactive noble gases is shown in Figure 3. The primary components which comprise the system are: (A and B) the cryostat containing the detectors and the sample chamber which are all cooled by liquid nitrogen, (C, D, E, and F) the gas handling and monitoring system, and, (G) the electronics for processing and analyzing the pulses from the two Si(Li) detectors.

The system as shown in Figure 3 permits the introduc-

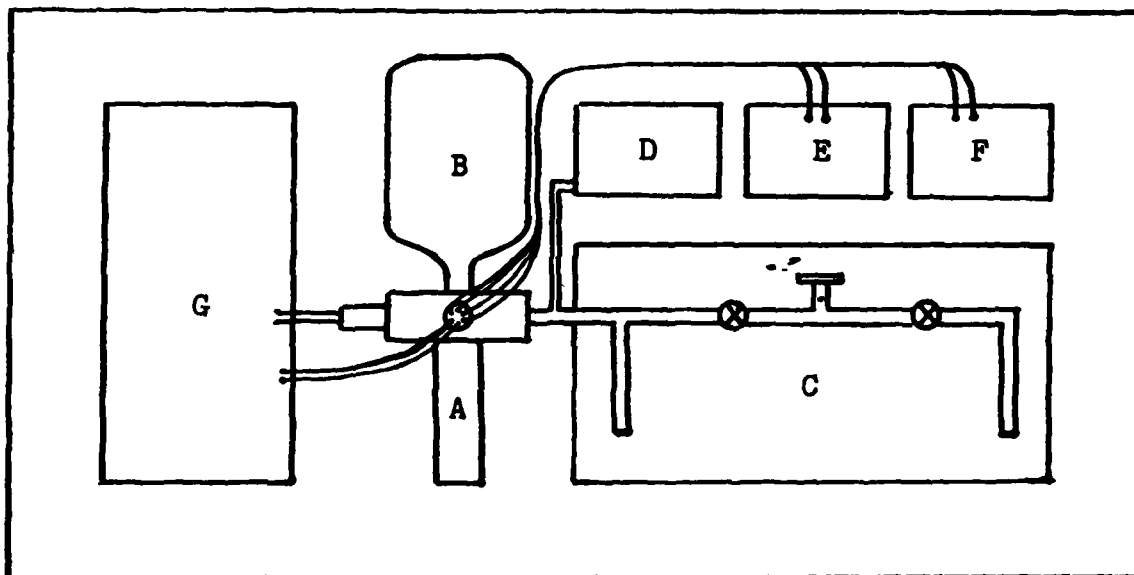


Figure 3. Total system components and general configuration. A is the stainless steel container where the detectors and sample chamber are located (See Figures 4 & 5). B is a "chicken-feeder" type reservoir for liquid nitrogen. C is the gas-handling system (See Figure 6), D is a pressure gauge, E a temperature gauge, and F a regulated DC power supply. G is the electronics for pulse processing and analysis (See Figure 7).

tion of various amounts of each radionuclide in addition to stable xenon to accomplish such analyses as sample "migration", x-ray fluorescence, self-absorption, reproducibility of results, detectors' efficiencies and resolutions, and determination of total activity by coincidence techniques.

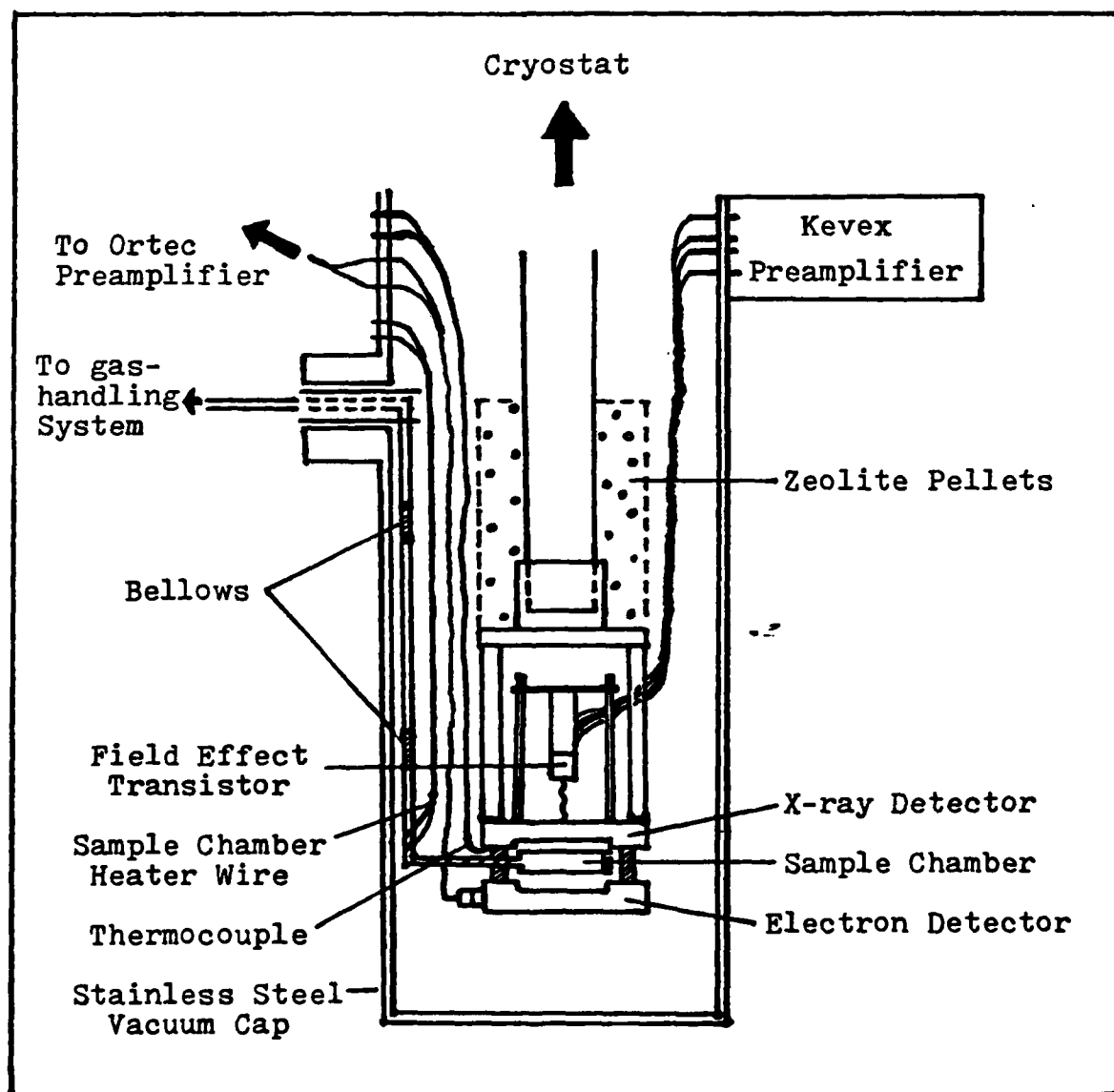


Figure 4. Cross-sectional View of Detection System Assembly.

Cryostat

A cross-sectional view of the detection system assembly is shown in Figure 4. The system is maintained at near liquid nitrogen temperatures by a "chicken-feeder" type reservoir which contains approximately a three-day supply of liquid nitrogen. The liquid nitrogen cools the detection system assembly through the use of a copper rod. The three significant differences between Hunt's (Ref 8) and that currently under study are: 1) the addition of a beryllium window "sandwich" to the sample chamber, 2) the addition of resistive heater wire windings around the sample chamber in addition to grounding improvements to minimize electronic noise and, 3) the addition of bellows to the sample chamber inlet pipe.

The first and most important design change was the removal of the 0.0635 cm beryllium window facing the x-ray

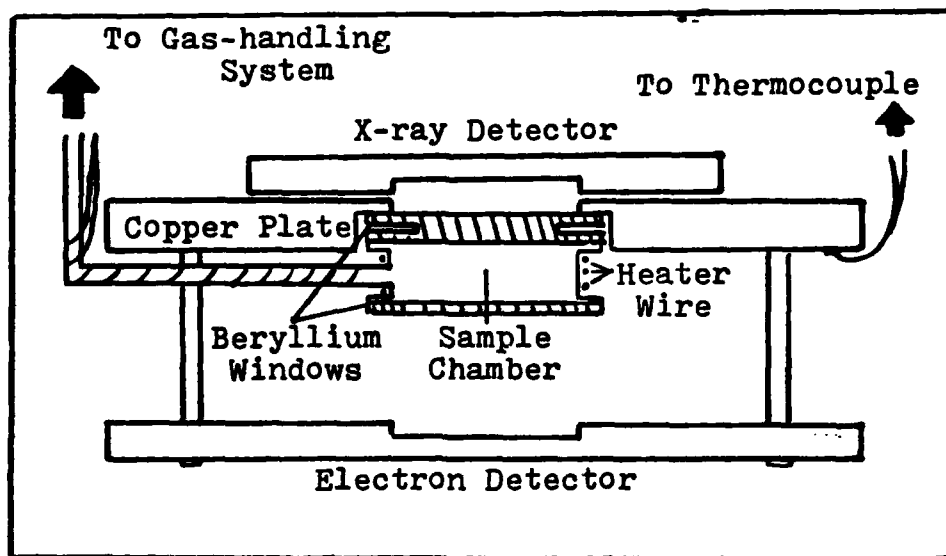


Figure 5. Detectors and Sample Chamber

detector and the replacement of it with a "sandwich" type of arrangement of three beryllium windows (Figure 5). The two outer windows have a diameter of 2.22 cm and the diameter of the middle window is 1.59 cm. They have a combined thickness of 0.12 cm. The intent of this modification was to ensure that the radioactive sample is deposited uniformly and reproducibly in the sample chamber. The design of the beryllium window "sandwich" is such that the coldest point in the sample chamber is the center of the beryllium window facing the x-ray detector and consequently a temperature gradient exists in all other directions. This temperature gradient is intensified by the application of heat to the wall of the sample chamber with a resistive heating wire which is coiled around the chamber. The heat flow starts at the middle of the window facing the x-ray detector, flows through the center window and then out radially through the outer beryllium window to an edge contact with the upper copper plate. The copper plate is coupled directly to the copper rod which is the base of the liquid nitrogen reservoir. More information is presented in Chapter V on this modification (in addition to the other two modifications) and the reasons for it (them).

The second modification to the detection system was the addition of resistive heating wire around the outside of the sample chamber. The temperature of the system is measured using a thermocouple (Figure 4) which is attached to the copper plate above the sample chamber. When 0.25 amps current

is applied to the 16 ohm resistive heating wire with a regulated DC power supply, it results in a 3°C increase in the temperature of the sample chamber. The intent of this modification was to minimize or eliminate the process of sample migration identified by Hunt (Ref 8). It also greatly facilitates the removal of the radioactive sample from the chamber. In addition, special attention was paid to the grounding of the various components of the system to minimize the large amount of electronic noise seen by Hunt.

Finally, the third major modification to the detection system involved the addition of two bellows to the stainless steel inlet pipe. The aim of this modification was to prevent stress on the bond (Figure 5) which holds the sample chamber to the copper heat sink. Prior to this design modification, thermal contraction produced stresses which resulted in the bond between the beryllium window and the copper plate to break. The addition of the two bellows inserts some flexibility into the system and compensates for the thermal contraction of the various components.

The final design of the sample chamber performs three very important functions. The first is to ensure that the radioactive sample is deposited uniformly and reproducibly in the sample chamber. This is accomplished by the unique design of the beryllium window sandwich which faces the x-ray detector ensuring that the coldest spot in the sample chamber is the center of the x-ray detector window and a temperature

gradient exists in all other directions. The second function of the sample-chamber design is to maximize the geometry factors of the two detectors. This is accomplished by having the chamber as thin as possible. This maximizes the window-to-total surface ratio and thus, the geometry factor for each detector is as close as possible to the theoretical limit of 0.5. The third function of the sample chamber is to allow one detector to detect both electrons and electromagnetic radiation while allowing the other detector to observe only electromagnetic radiation. This is done by simply varying the thickness of the beryllium windows facing each detector. The relatively thinner beryllium window facing the electron detector allows the transmission of both electromagnetic radiation and electrons whereas the much thicker window facing the x-ray detector allows the transmission of only electromagnetic radiation. The 0.12 cm window facing the x-ray detector stops all electrons with energies less than 450 keV (Ref 16). On the other hand, the much thinner window of the electron detector (0.0015 cm) permits transmission of all electrons with energies in excess of 35 keV.

Gas-handling and Measuring Equipment

The gas-handling system is a series of sections of stainless steel tubing separated by Nupro valves and is shown in Figure 6. It consists of 1) eight valves (V1 - V8), 2) a sample chamber, 3) a diffusion pump to evacuate the system, 4) a pressure gauge (G), 5) two cold fingers (F1 and F2),

6) two locations for attaching a breakseal tube (H1 and H2), and 7) a 5-liter bottle of stable xenon.

A gas sample is received in a glass tube equipped with a breakseal and is connected at one of the two locations in the system for attaching breakseal tubes. The portion of the gas to be counted is cryogenically transferred to a calibrated volume which is attached to a pressure gauge and the remainder is either left in the breakseal or cryogenically transferred to a cold finger for storage. In addition, a five liter bottle of stable xenon is connected to the gas-

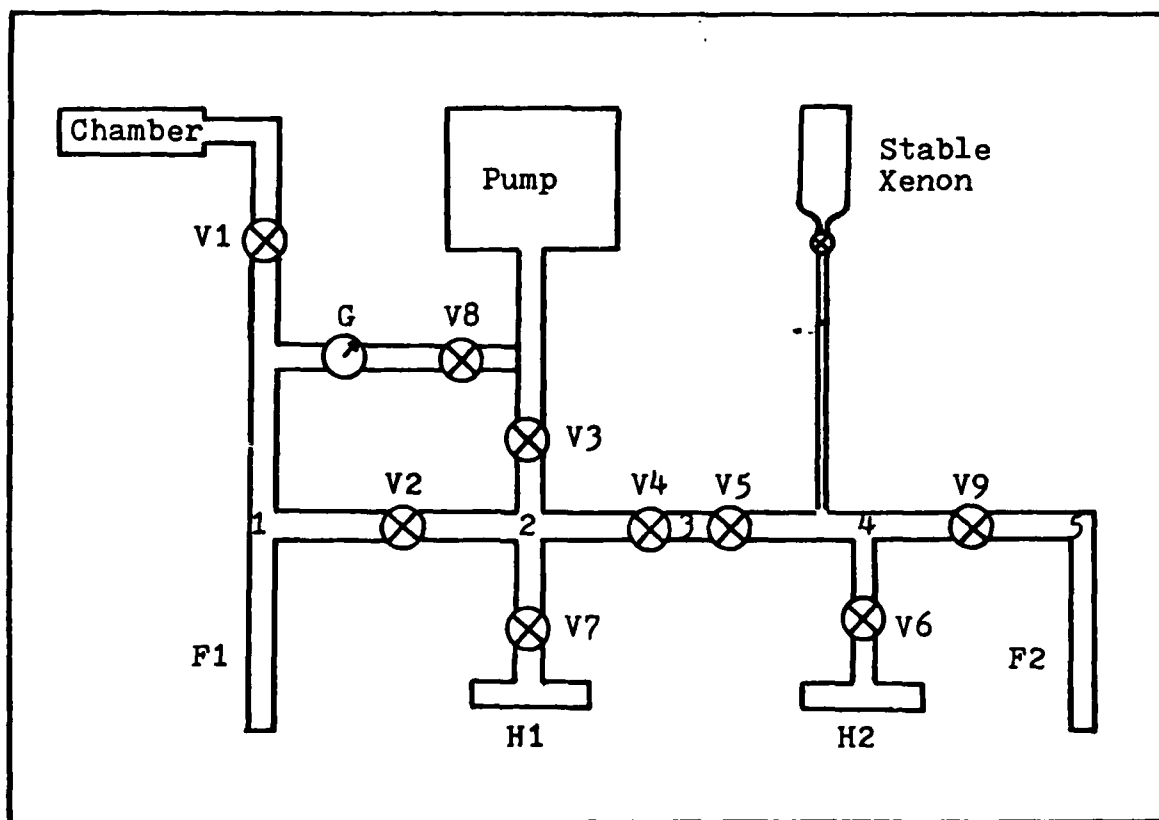


Figure 6. Gas-handling System

handling system by a piece of plastic tube. Thus, any desired combination of the two radioisotopes may be prepared for entry into the sample chamber. Again by cryopumping, the known quantity of sample is transferred to the sample chamber in the cryostat. When the condensation site of the sample has finally stabilized, the analysis may begin.

The xenon sample is removed from the sample chamber by applying liquid nitrogen to one of the two cold fingers in the gas-handling system. Additionally, a regulated DC power supply is used to provide 0.25 amps of current to a resistive heating wire which is coiled around the sample chamber. This serves to warm the chamber approximately three degrees centigrade and thus forces the xenon out of the chamber at a much faster rate. The entire system is evacuated to about 10^{-6} Torr with a diffusion pump.

Detectors and Their Characteristics

Both detectors are lithium-drifted silicon (Si(Li)) semiconductors, manufactured by Kevex Corporation and have an active area of three square centimeters. The x-ray detector has a sensitive depth of 0.5 cm and is maintained at near liquid nitrogen temperatures by a direct connection to the copper cryostat rod. A field-effect transistor (FET) is mounted directly below the detector to minimize the electronic noise. The electron detector has a sensitive depth of only 0.2 cm thus making it much less efficient for electromagnetic radiation but thick enough to stop 1500 keV electrons. In

addition to those modifications already mentioned, one additional modification was made with respect to the positioning of the electron detector. In Hunt's system, the electron detector was cooled by edge contact with the sample chamber. In an effort to establish a temperature gradient across the sample chamber, the electron detector was moved a short distance (about 0.1 cm) away from the sample chamber. The electron detector is now cooled solely by a copper rod connected to the cryostat rod.

Electronics for Pulse Processing and Analysis

A block diagram representing the electronics which were used for pulse processing and analysis in this study can be seen in Figure 7. An Ortec Power Supply provides a negative bias of 600 volts to the x-ray detector. As previously mentioned, a field-effect transistor (FET) is mounted inside of the cryostat directly above the detector. The remainder of the preamplifier is mounted externally to the stainless steel vacuum cap. A Kevex linear amplifier is then used to shape and amplify the pulse. A positive bias of 375 volts is applied to the electron detector by a Nuclear Electronics Power Supply. The pulses from the electron detector are processed by an Ortec preamplifier and then shaped and amplified by an Ortec linear amplifier.

The monopolar signals from the two linear amplifiers are fed into two Tennelec Timing Single Channel Analyzers (TSCA). The TSCAs are used to select part, or all, of the

energy spectrum of the radioisotopes. The TSCAs provide a logic signal output to a gate and delay generator whose output pulse is then used in conjunction with a Multichannel Analyzer (MCA) to gate an input signal from the linear amplifier (Figure 7). In addition, the output signals from the TSCAs can be used in coincidence analysis as the start and stop signals for a Time-to-Amplitude Converter (TAC) which in turn produces an output pulse whenever the two TSCA's pulses arrive within a preset resolving time. Two Multichannel Analyzers are used, both of which are linked to a plotter for hard copy plots and a teletype for a read-out of data. The MCAs can be used to obtain a pulse height spectrum from each detector individually or to obtain a time spectrum from the TAC for analysis.

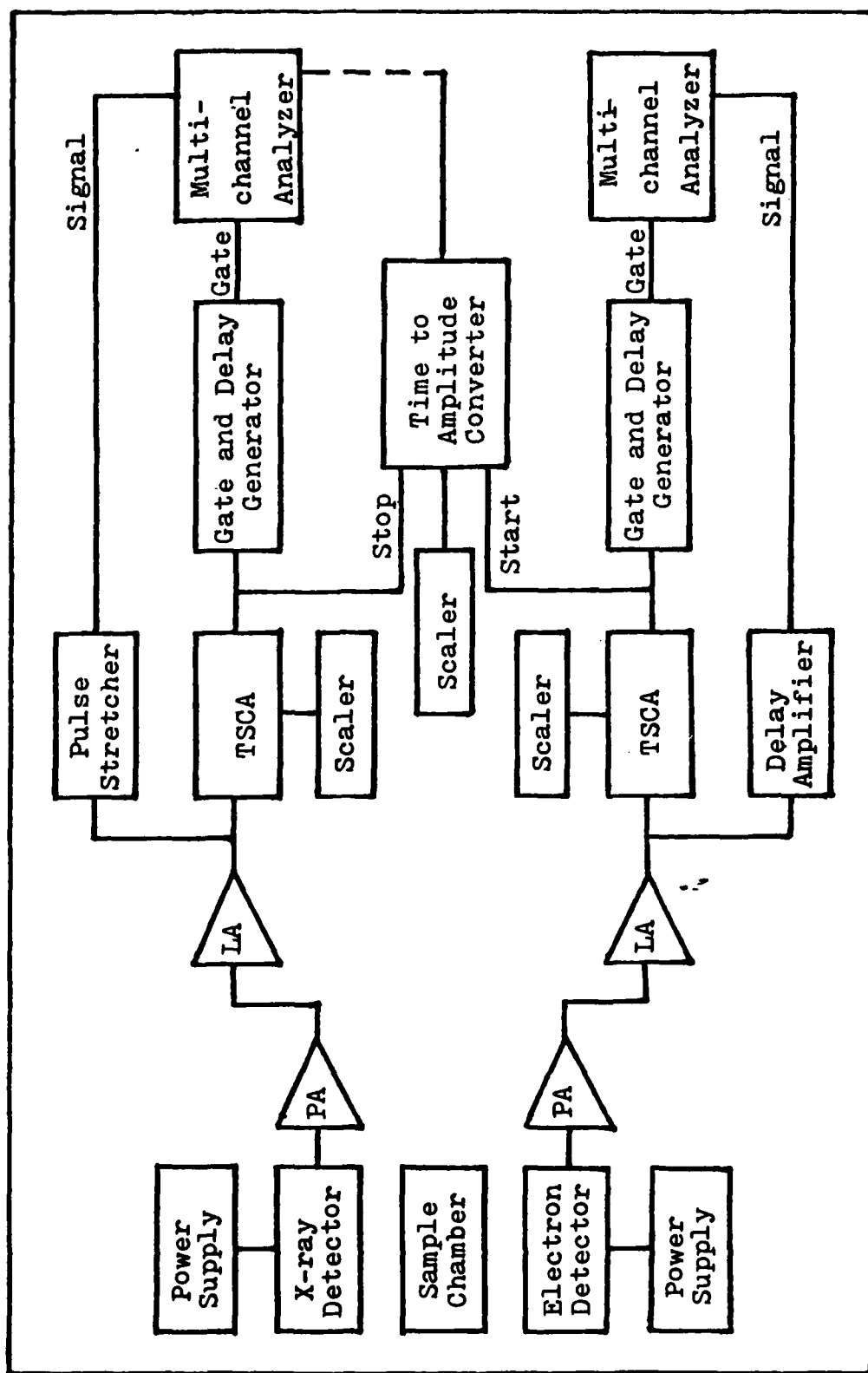


Figure 7. Basic modular system for the use of TSCAs for the setting of energy spectrum 'windows' and using resultant signal to gate the MCA with the output from the respective linear amplifier as the input signal to the MCA. The TAC can be used for coincidence analysis and the time spectrum can be observed with the MCA.

IV. Time To Amplitude Converter and Coincidence Counting

Purpose

The primary reason for using a Time To Amplitude Converter (TAC) and coincidence techniques in this study was to experimentally determine the activity of ^{131m}Xe . The radiations of ^{131m}Xe which were used for the coincidence analysis are the internal conversion electrons and the characteristic xenon x rays. In addition, the TAC was used to determine whether the xenon carrier gas x-ray fluorescence was a result of the high energy beta particles of ^{133}Xe or if the fluorescence was a result of some other nuclear process.

Time To Amplitude Converter (TAC)

A Time To Amplitude Converter can be used when fast coincidence requirements are needed. A TAC is a device which produces an output pulse whose amplitude is linearly proportional to the time interval between a start input and a subsequent stop input. When a start input is seen by the TAC it begins the charging of a capacitor by a constant current source. This charging process continues until either a stop signal is seen or until a preset resolving time elapses. If a stop pulse is observed prior to the resolving time elapsing, an output pulse is generated which is proportional to the time interval between the start and stop pulses. The TAC is then ready to accept another start pulse. The TAC not only indicates when two events are in coincidence but also will tell how events are distributed with respect to time.

Chance Coincidences

A chance coincidence occurs when two pulses (not coincident) arrive at the TAC at the respective start and stop inputs within the resolving time, t , of the TAC. The rate at which chance coincidences occur is a function of the single's rate of each branch (m_x and m_e) and the resolving time (t) of the system. The chance coincidence rate is given by (Ref 1:322)

$$m_c = b_c + 2tm_x m_e \quad (1)$$

Background produced by a single cosmic ray particle penetrating both detectors is represented by b_c . Generally, this is insignificant and can be ignored.

Bueler (Ref 1:323) states that it is desirable that the chance coincidence rate be smaller than the true coincidence rate. This imposes a limitation on the source strength S because the true coincidence rate increases proportionally with S , whereas the chance coincidence rate increases proportionally with S^2 . For example, the electron detector and x-ray detector counting rates are

$$m_e = S\epsilon_e \quad (2)$$

$$m_x = S\epsilon_x \quad (3)$$

where ϵ_e and ϵ_x are the probabilities of detecting an electron in the electron detector and an x ray in the x-ray detector, respectively. The number of true coincidences is simply the product of the probabilities times the source

strength, or

$$m_{ex} = S\epsilon_e\epsilon_x \quad (4)$$

The chance coincidence rate is

$$m_c = 2tm_em_x = 2tS^2\epsilon_e\epsilon_x \quad (5)$$

and our limiting condition of $m_c < m_{ex}$ becomes

$$2tS < 1 \quad (6)$$

For the 40 μ second resolving time used in this study, the source strength is limited to 1.25×10^4 decays per second.

Time Spectrum

Figure 8 represents a typical multichannel analyzer's time spectrum for a radioactive source emitting radiation in coincidence. One quickly sees how similar the time spectrum is to an energy spectrum. The cross-hatched area represents the total number of true coincidence counts. The prompt coincidence peak has a full width at half maximum (FWHM) which is normally referred to as the time resolution of the system. The FWHM indicates the total contribution of all electronic sources to timing uncertainties. If the detectors, electronics, and triggering conditions in both electronic branches are nearly identical, then the prompt coincidence peak should be symmetric. Conversely, if one of the branches is significantly different from the other, an asymmetric peak will result. The effect of amplitude walk in leading edge triggering can produce a number of pulses which occur much later

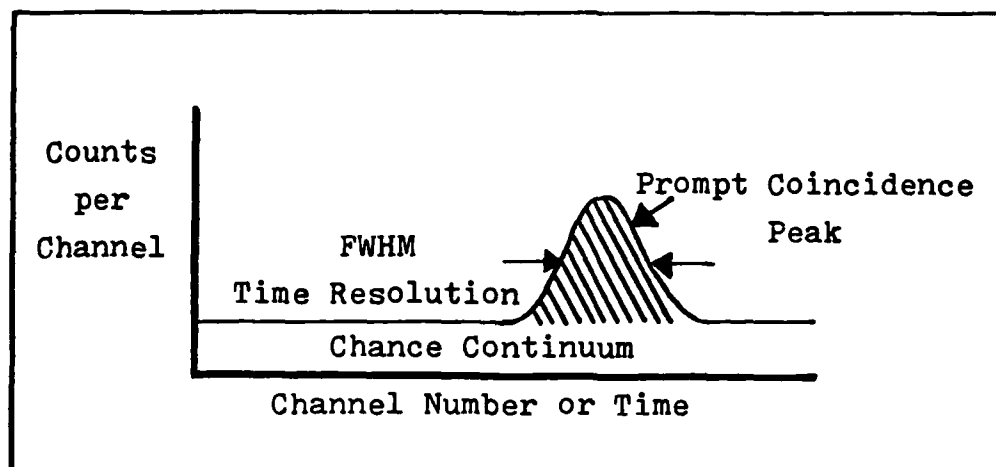


Figure 8. Multichannel Analyzer Time Spectrum.
(Ref 10:690)

than the majority. One can see from Figure 8 that the chance coincidence continuum is uniform over the entire time spectrum. This will always be true so long as the singles rates are not large relative to the inverse of the resolving time of the TAC. The chance coincidence rate per channel is the product of the singles rates and the time width (T) per channel on the MCA or $m_e m_x T$ (Ref 10:691).

Measurement of Source Activity and Detector Efficiencies

Coincidence techniques can be used to calculate the gross activity of a source without any knowledge of the detector's efficiencies (Ref 10:699). The source activity can be measured by knowing the singles rates of the two detectors in addition to the coincidence counting rate. Let S be the true activity of the source, m_e and m_x the singles rates for the electron and x-ray detectors respectively and ϵ_e and ϵ_x the total efficiencies of each detector. Then the singles

rate can be expressed as

$$m_e = \epsilon_e S \quad (7)$$

$$m_x = \epsilon_x S \quad (8)$$

and the measured coincidence as

$$m_{ex} = \epsilon_e \epsilon_x S + m_c \quad (9)$$

where $\epsilon_e \epsilon_x S$ is the true coincidence rate and m_c is the chance coincidence rate. Solving Eqs (7), (8), and (9) simultaneously and eliminating ϵ_e and ϵ_x we find

$$S = \frac{m_e m_x}{m_{ex} - m_c} \quad (10)$$

Now that S is known, the efficiencies for each detector can be calculated by the use of Eqs (7) and (8).

Experimental Applications

The activity of the ^{131m}Xe sample and the efficiencies of the x-ray detector for the various radiations of ^{131m}Xe and ^{133}Xe were calculated by the use of or with Eqs (7), (8), and (10). The output of the electron detector's TSCA was used as the start input to the TAC and the signal from the x-ray detector's TSCA was used as the stop input. Due to the dissimilarities between the electronics of the two branches, the resolving time of the TAC had to be set at a relatively high value of 40 μ seconds.

V. Factors Affecting Detection

Introduction

There are six principal factors which affect the detection and measurement of radioisotopes using the detection system under evaluation in this project. These factors are 1) sample migration, 2) sample self-absorption, 3) carrier gas fluorescence, 4) geometry, 5) detector efficiencies, and 6) detector resolutions.

Migration

Hunt (Ref 8) found sample migration to be a significant problem in this detection system prior to its modification. He hypothesized that the sample was migrating from the beryllium windows to the rim of the sample chamber. This process resulted in a large amount of scattering of the internal conversion electrons of ^{131m}Xe and a lower efficiency due to a change in the geometry factor.

As explained in Chapter III, the principal intent of the modification to the beryllium window facing the x-ray detector and of the addition of the resistive heating wire was to make the center of the beryllium window facing the x-ray detector the coldest point in the sample chamber. The improved design accomplished this through the establishment of a temperature gradient in all directions away from that point. This temperature gradient is intensified by the resistive heating wire depositing approximately one watt of heat to the walls of the sample chamber. These modifications

did not eliminate the problem of sample migration but they did speed up the migration process from approximately 24 hours to 2½ hours. In addition, the xenon can now be deposited in the center of the beryllium window facing the x-ray detector in a predictable, uniform, and reproducible manner.

Self-Absorption

If a radioactive sample is not infinitely thin, then the observed count rate may be different from the actual count rate by a factor, f_s , due to 1) an increase in the number of particles reaching the detector as a result of scattering within the source in the direction of the detector and, 2) a decrease in the observed count rate due to absorption of radiation by the source (Ref 1:86). Ideally, a source should be made thin enough so that these effects may be ignored. If this is not possible, then a self-absorption factor, f_s , must be calculated to take into account the effect of the finite thickness of the source on the number of particles being detected (Ref 17:132). For small source to detector distances (as in this system), the scattering effect may be ignored (Ref 17:133).

The self-absorption factor is a function of the thickness of the source, s , and can be calculated if we ignore scattering and assume an exponential absorption with a total absorption coefficient, μ . If the source has an activity of c_0 in the direction of the detector if self-absorption is neglected, then the activity due to a thin layer dx is

$$dc_o = \frac{c_o}{s} dx \quad (11)$$

The activity which escapes the source from a layer at a distance x from the surface can be assumed to be reduced by a factor of $e^{-\mu x}$ and thus

$$dc = \frac{c_o}{s} \cdot e^{-\mu x} \cdot dx \quad (12)$$

and if we integrate dc over the entire thickness of the source we find

$$c = \int_0^s dc = \int_0^s \frac{c_o}{s} \cdot e^{-\mu x} \cdot dx = \frac{c_o}{s} (1 - e^{-\mu s}) \quad (13)$$

and

$$f_s = \frac{c}{c_o} = \frac{1}{\mu s} (1 - e^{-\mu s}) \quad (14)$$

Table VII shows the calculated theoretical self-absorption factors for the various radiations of interest along with the observed experimental values.

Carrier Gas Fluorescence

Carrier gas fluorescence is caused by a gamma ray or electron from either ^{131m}Xe or ^{133}Xe striking a carrier gas atom and depositing enough energy to remove an orbital electron from the atom (34.566 keV is required for a K shell electron of xenon). The atom now exists in an excited state which lasts approximately a nanosecond or less (Ref 10:21). The atom then de-excites through the rearrangement of its electrons which results in the emission of a characteristic

xenon x ray whose energy is equal to the energy difference between the electron's initial and final energy states. These fluorescence x rays are indistinguishable from the xenon characteristic x rays which are given off as a result of the internal conversion process of ^{131m}Xe . It is obvious from this that the fluorescence process must be quantified if x-ray spectroscopy is to be used to identify and quantify the decay of ^{131m}Xe in the presence of ^{133}Xe .

The samples which were used for analysis contained significant quantities of xenon carrier gas. The ^{133}Xe sample contained over 50 billion atoms of the carrier gas for every ^{133}Xe atom and for the ^{131m}Xe sample the ratio was over 30 billion to one. Thus, for subsequent analysis it will be assumed that the sample consists entirely of xenon carrier gas.

Geometry

The geometry factor, f_g , is generally defined to be the fraction of the source radiation which is incident on the detector face and can be represented by

$$f_g = \frac{\Omega}{4\pi} \quad (15)$$

where Ω is the solid angle subtended by the detector at the source position. The solid angle is the integral over the face of the detector of the form

$$\Omega = \int_A \frac{\cos \theta}{r^2} dA \quad (16)$$

where r is the distance between the source and a surface

element dA , and θ is the angle between its normal and the source direction. It was determined experimentally that the source was depositing itself in a very small area (6.74×10^{-3} cm) and thus, the simplifying assumption of a point source on axis with a disc detector could be made. With this assumption, Eq (16) reduces to

$$\Omega = 2\pi(1 - \cos \theta) \quad (17)$$

The distances from the source to the x-ray and electron detectors are 0.1 cm and 0.7 cm respectively. For a detector radius of 0.977 cm, the geometry factor for the x-ray detector computed with Eq (17) is 0.449 and for the electron detector it is 0.209.

Detector Efficiencies

The intrinsic photopeak efficiencies of the two detectors for the electromagnetic energies of interest are shown in Table V. This table shows how the intrinsic photopeak

Table V
Detector Intrinsic Photopeak Efficiencies
For Electromagnetic Radiation

Detector	Thickness (mm)	Energy (keV)	Efficiency
X ray	5	30	0.63
Electron	2	30	0.40
X ray	5	81	0.049
Electron	2	81	0.022

(Ref 21)

efficiencies of semiconductor detectors are a strong function of the energy of the incident radiation and the detector thickness. The intrinsic efficiencies for both detectors for electrons with energies less than 350 keV approaches 100%.

The 1.52×10^{-3} cm thick beryllium window facing the electron detector has an insignificant effect on the electromagnetic energies of interest but the 129 keV internal conversion electrons of ^{131m}Xe deposit 8.38 keV of energy in the window and 7.32 keV is deposited by the 158 keV internal conversion electrons (Ref 16:12). The 0.102 cm beryllium window which faces the x-ray detector completely stops all electrons of energies of interest in this study and attenuates the characteristic x rays of xenon and cesium (about 30 keV) by approximately 3.3%. The 81 keV gamma of ^{133}Xe is attenuated by 2.6% (Ref 13:17).

Resolution

The principal contributors to the spectral resolution of the detectors in this study are 1) noise attributed to the individual signal processing branches and, 2) spread due to charge generation statistics. Electronic noise was the determining effect in this study.

The full width at half maximum (FWHM) of the full energy peak W_t (Ref 10:480) can be represented as

$$W_t = \sqrt{W_e^2 + W_d^2} \quad (18)$$

where W_e is the electronic noise and W_d is the spread due to charge generation statistics. W_d can be represented by

$$W_d = 2.35 \sqrt{F \epsilon E} \quad (19)$$

where F is the Fano factor (0.1), ϵ is the energy required to create one electron hole pair (3.76 eV) and E is the energy of the radiation of interest (Ref 10:363). Table VI shows the observed values for W_t and the calculated values for W_d and W_e for the various electromagnetic radiations of interest. It is obvious from this table that the most significant contributor to spectral resolution in this system is electronic noise.

Table VI
Detector Resolutions

Detector	W_d (keV)		W_e (keV)		W_t (observed) (keV)	
	81keV	30keV	81keV	30keV	81keV	30keV
X ray	0.175	0.106	0.597	0.564	0.772	0.670
Electron	0.175	0.106	---	4.448	---	4.554

VI. Data Analysis and Results

Introduction

The experimental results of this research are presented in this section. First the experimental results pertaining to sample migration, self-absorption, and carrier gas fluorescence are analyzed. Next, background radiation and time spectroscopy are discussed and finally sample energy spectra characteristic of both radioisotopes are presented.

Migration

Figure 9 shows how for early times (less than $2\frac{1}{2}$ hours) the electron detector shows a decrease in activity which is much more rapid than the normal decay of ^{131m}Xe would indicate. The x-ray detector indicates no sign of any migration

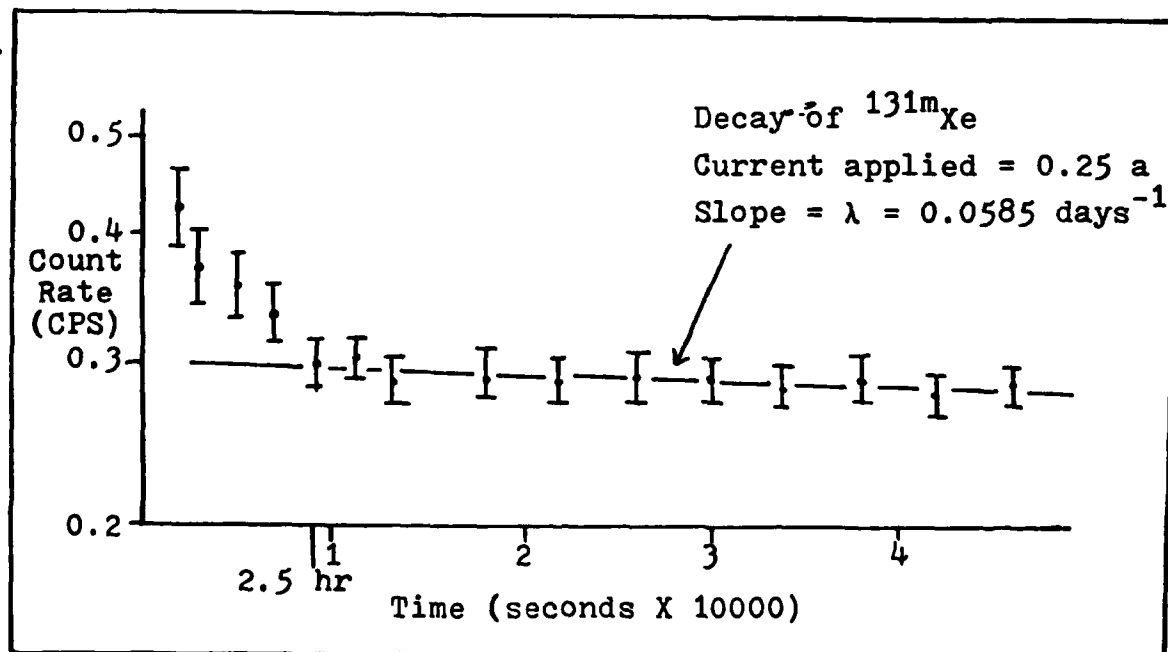


Figure 9. Count Rate Decrease After the Admission of Sample to Chamber.

taking place but simply decays exactly as ^{131m}Xe 's decay constant would predict. The reason for this is that the electron detector is much more sensitive to geometry than the x-ray detector because of its' being approximately 7 mm away from the final deposition area of the sample whereas the x-ray detector is only 1 mm away. This large decrease in activity seen by the electron detector is caused by the manner in which the sample gas is initially deposited in the sample chamber.

Initially, the sample gas deposits on all surfaces of the chamber since all are at a temperature below the freezing point. Then it migrates to the coldest point in the sample chamber which is where its vapor pressure is lowest. This is the center of the window facing the x-ray detector because of the heat transfer path and the heating of the cylindrical wall of the chamber. Eventually, temperature equilibrium is established, migration ceases and all of the condensed gas is presumed to be localized at the center of the window facing the x-ray detector.

This process dramatically changes the geometry factor associated with the electron detector resulting in lower count rates, lower efficiency, and poorer resolution. These are all negative results of the migration process. The one positive aspect is that finally this process can be controlled and speeded up so that the migration time is now a more reasonable $2\frac{1}{2}$ hours rather than the previous 24-36 hours. The time associated with the migration process is a function of the amount of current applied to the resistive heating

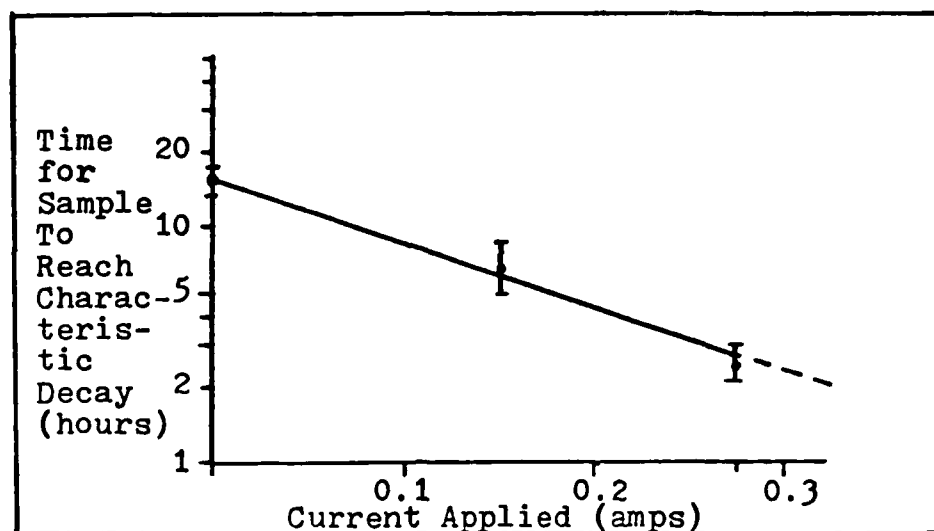


Figure 10. Time for Sample to Reach Its Characteristic Decay vs Heater Current Applied.

wire. As shown in Figure 10, the migration time decreases linearly with respect to the amount of current through the resistive heating wire. In addition, in order for the xenon to be deposited in a uniform and predictable manner, the heater must be left on at a constant heating level throughout any given experiment. This insures that the xenon will deposit itself in the same amount of area on the x-ray window and thus such factors as self-absorption, carrier gas fluorescence, and geometry will remain constant for any given experiment.

Self-Absorption

Price (Ref 17) suggests that the self-absorption factor, f_s , should be determined as a function of the sample thickness, s , for the particular arrangement used. This was accomplished by making a series of measurements while maintain-

ing constant activity for the source (^{131m}Xe) and increasing the sample thickness by the addition of inactive material (stable xenon). The experimental values for f_s and Eq (14) were used to determine the deposition area of the sample ($6.740 \times 10^{-3} \pm 0.270 \times 10^{-3} \text{ cm}^2$), and then the theoretical values of f_s were calculated. The values of 0.04174 gm/cm^2 and 0.05714 gm/cm^2 were used for μ for the 129 keV and 159 keV internal conversion electrons, respectively (Ref 16). The total absorption crosssection for the xenon x rays was computed to be $8.888 \text{ cm}^2/\text{gm}$ (Ref 13). Figure 11 demonstrates how the total x ray counts decreased in an exponential manner as a function of sample thickness. Table VII shows the experimental and theoretical values for f_s . The theoretical

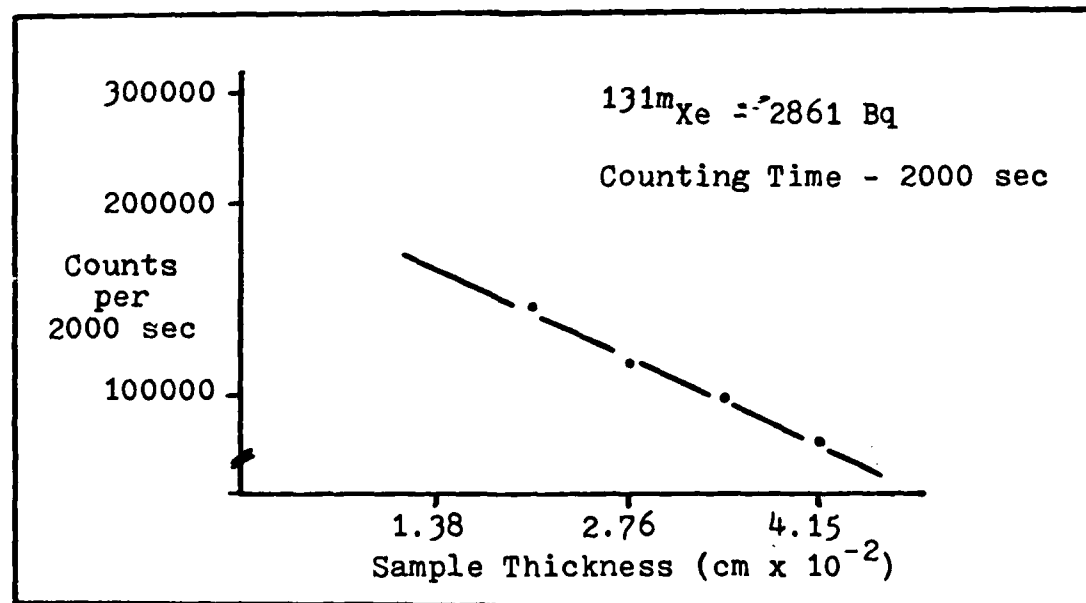


Figure 11. Self-Absorption of Xenon-131m Internal Conversion Electrons.

Table VII
 ^{131m}Xe Self-Absorption Factors

Sample Thickness (cm)	Electron Self-Absorption Factors		X-ray Self-Absorption Factors	
	Theory	Experiment	Theory	Experiment
0.01383	0.615	0.635	0.811	0.957
0.02075	0.500	0.521	0.734	0.883
0.02766	0.415	0.435	0.668	0.843
0.03457	0.351	0.370	0.610	0.826
0.04149	0.302	0.319	0.558	0.803

and experimental values for the internal conversion electrons agree very well but the x-ray values differ significantly. This is principally because there are two competing effects taking place. One is self-absorption and the other is carrier gas fluorescence. Thus, the experimental values are significantly higher than the theoretical values. In fact, the differences increase linearly as a function of the sample thickness in the same manner we would expect the number of fluorescent x rays to increase.

When the same experiment was performed with ^{133}Xe , the results were significantly different for the electron count rate as a function of sample thickness. It was found to increase as stable xenon was added and the source thickness increased. This result was a function of the electron detector's energy 'window' being set at 85 keV and 175 keV.

What was happening was that self-absorption was causing more of the beta particles with energies greater than 175 keV to be degraded in energy so that they now have an energy bracketed by the electron detector's energy window then are being "self-absorbed" out of the electron detector's energy window. Thus, a resultant increase in the electron count rate. As far as the x-ray count rate was concerned, again, the two competing effects of self-absorption and carrier gas x-ray fluorescence were present. Although self-absorption was theoretically taking place, the fluorescence effect was dominant due to the increased amount and energy of the beta particles (relative to the internal conversion electrons of ^{131m}Xe) in the sample.

Finally, the self-absorption effect associated with this system can be minimized by simply admitting the sample to the sample chamber and waiting the 24 to 36 hours for the sample to complete its migration process without any (or very little) heat being applied to the sample chamber. In this way the area over which the sample is deposited is maximized and the thickness of the sample is minimized. The actual deposition area can be found by repeating the experiment described above, experimentally determining the self-absorption factors and using Eq (14) to find the thickness of the sample. Knowing the amount of sample deposited, one can then determine the area over which it was deposited.

Carrier Gas Fluorescence

Carrier gas fluorescence is a function of 1) the deposition thickness of the sample, 2) the type and energies of the various radiations in the sample and, 3) the activity of the sample. In this study it was possible to experimentally determine the amount of carrier gas fluorescence with both the ^{131m}Xe and the ^{133}Xe . Separate experiments were performed for each radioisotope. Fluorescence was quantified by making a series of measurements while maintaining a constant activity for the source and increasing the sample thickness by the addition of stable xenon. Figure 12 shows how the carrier

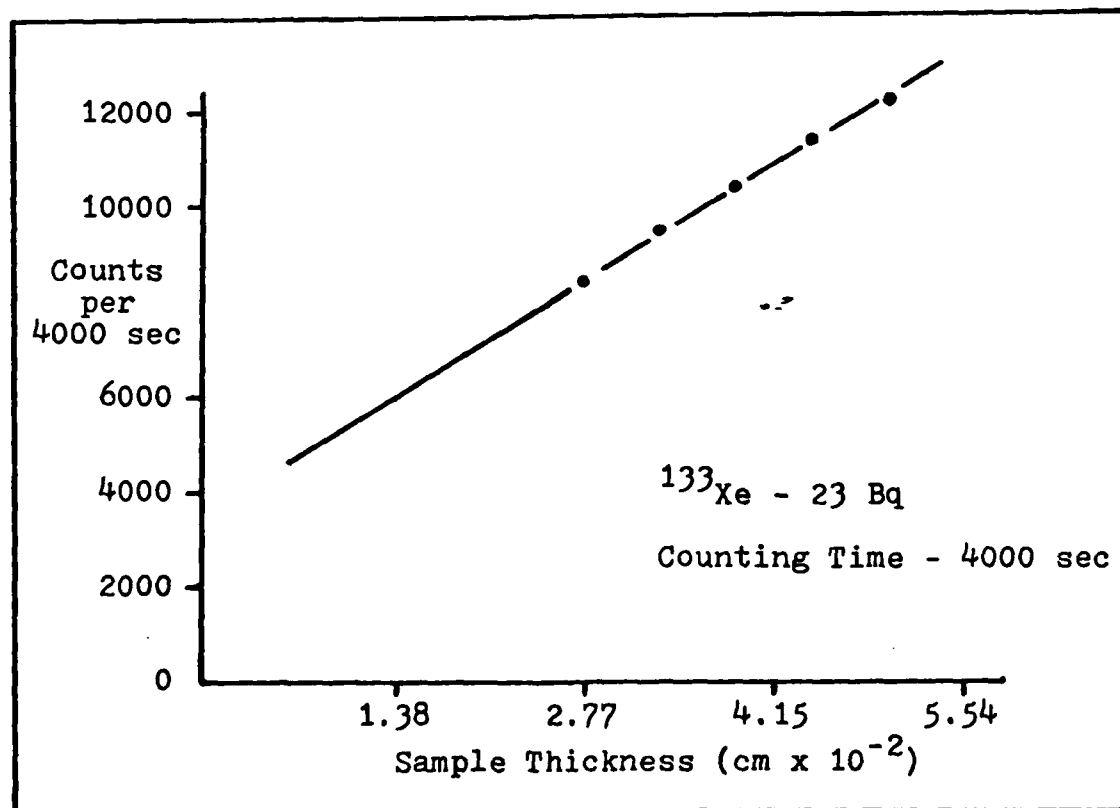


Figure 12. Xenon-133 Carrier Gas X-ray Fluorescence.

gas x-ray fluorescence increased in a linear manner. Applying a linear least squares fit to the data resulted in a value of 0.173 ± 0.015 fluorescence x rays per second for each increase of 2.77×10^{-4} cm in the thickness of the ^{131m}Xe sample with a constant activity of 2885 Bq. For the ^{133}Xe sample an increase of 0.0116 ± 0.0010 fluorescence x rays per second was observed for the same increase in source thickness with a constant activity of 23 Bq. Although the rate of increase of the ^{133}Xe sample was much less than that of the ^{131m}Xe sample, if we assume that carrier gas scales linearly with sample activity, we find that the ^{133}Xe sample produces 8.40 times as many fluorescence x rays as does the ^{131m}Xe sample per unit of sample activity. This result is caused principally by the more abundant and more energetic beta particles of ^{133}Xe .

Background

Natural background radiation was determined with the system configured as it would be for an actual sample analysis. Passive shielding of approximately three inches of lead is used to reduce much of the natural background caused by the progeny of uranium and thorium which may be present in the construction materials of the laboratory. This shielding is also effective against secondary radiations caused by cosmic ray interactions in the atmosphere (Ref 10:779). Background runs of forty thousand seconds were taken for each detector. No significant peaks were observed in the

energy spectrum of either detector and the background radiation level was $1.27 \times 10^{-3} \pm 0.02 \times 10^{-3}$ Bq /keV from 26.5 keV to 36.3 keV for the x-ray detector and $3.42 \times 10^{-4} \pm 0.10 \times 10^{-4}$ Bq/keV from 85 to 175 keV for the electron detector.

Time Spectroscopy

A typical experimental time spectrum is shown in Figure 13. This was generated by the Time to Amplitude Converter (TAC) with the electron detector branch as the start signal and the x-ray detector branch as the stop signal. The FWHM was calculated to be 0.62 μ seconds and the time width per channel was 0.0488 μ seconds. A slight skewing to the higher time channels can be observed in the time spectrum. This is caused by the dissimilarities in the two electronic branches. Leading edge triggering is used throughout this study and the effects of amplitude walk cause a small number of the pulses

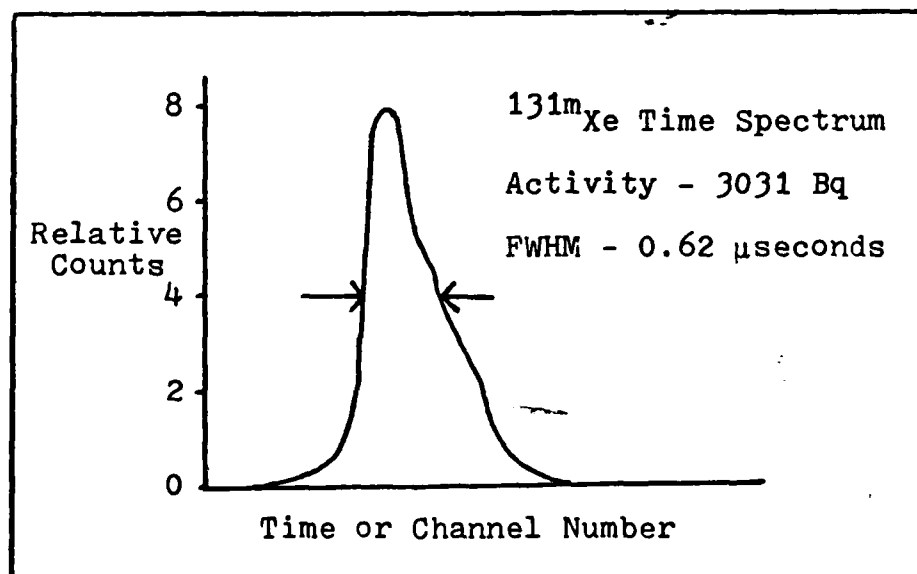


Figure 13. Xenon-131m Time Spectrum

to occur substantially later than the majority.

In addition to determining the activity of the ^{131m}Xe sample, the TAC was used to insure that the carrier gas fluorescence in ^{133}Xe was in fact being caused by the beta particles exciting carrier gas atoms and not some other nuclear process. This was accomplished by setting the x-ray detector's TSCA so that all radiations were being discriminated against except the K_{β_2} x rays of cesium. The TSCA was set so that electrons of energies 85 to 175 keV were being observed. A 4000 second count resulted in no time spectrum being observed or any coincident counts being recorded whereas when the x-ray detector's TSCA was set to discriminate against all radiation except the K_{α} x rays of xenon, the result was a time spectrum very similar to that in Figure 13. Thus, the carrier gas x-ray fluorescence observed with ^{133}Xe was, in fact, due principally to the abundant and highly energetic beta particles associated with the decay of ^{133}Xe .

Xenon-131m Energy Spectra

Figure 14 is an energy spectrum of ^{131m}Xe which is typical of those obtained with the electron detector during this study. Two problems are easily identified from this spectrum: 1) The low energy tailing of the internal conversion electron peaks due to self-absorption, and 2) The background level due to scattering of the internal conversion electrons (between the x-ray peak and the internal conversion electron peaks). Both the efficiency of the electron detector

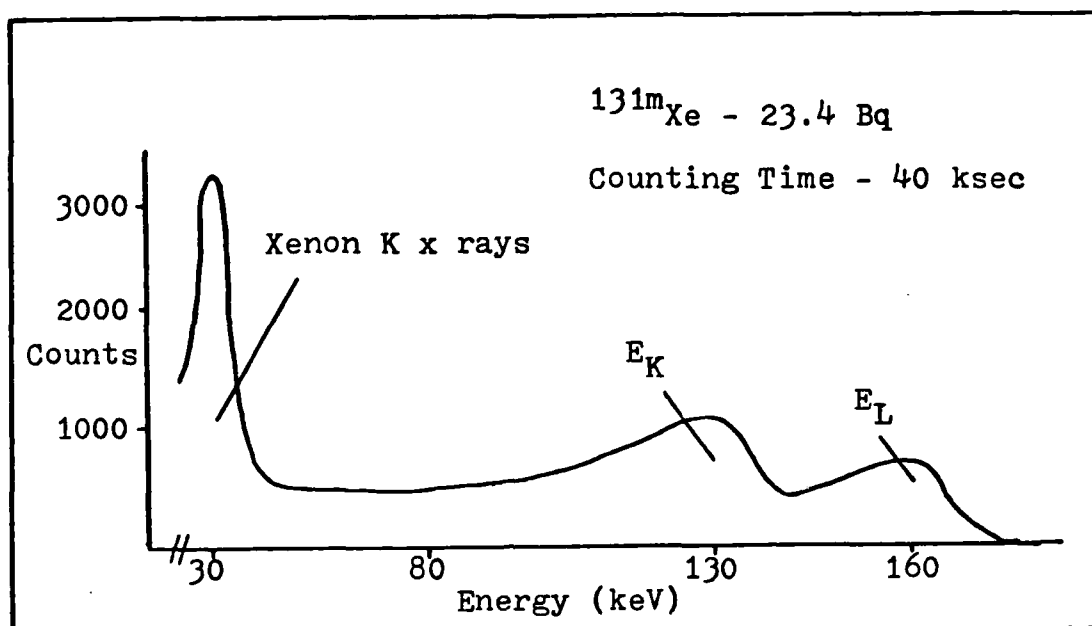


Figure 14. Xenon-131m Electron Energy Spectrum

and the resolution of the internal conversion electron full energy peaks are strongly related to the amount of xenon in the sample chamber. The resolution for the 129 keV peak was calculated with the assumption that the lower energy side of the peak was symmetric to the higher energy side. The best resolutions (as measured by FWHM) observed with this detector were 6.6, 10.0 and 9.2 keV for the K shell x rays, the 129 keV and the 159 keV internal conversion electron peaks respectively. This was measured with only 0.011 cc of xenon in the sample chamber. When the amount of xenon was increased to 0.22 cc, the resolution for the internal conversion electron peaks increased to 32.6 and 19.2 keV respectively. A total efficiency of only 0.551% was calculated for the 159 keV peak with 0.111 cc of xenon in the sample chamber. Although these results are a large improvement over Hunt's (Ref 8), it ap-

appears unlikely that electron spectroscopy can be used to identify and measure $^{131\text{m}}\text{Xe}$ in the presence of ^{133}Xe .

Figure 15 shows a typical energy spectrum obtained with the x-ray detector with $^{131\text{m}}\text{Xe}$ as the radioactive source. It is obvious that the two K_{α} peaks (29.458 and 29.779 keV) cannot be resolved but that the K_{β} peaks are, in fact, resolved. The best resolutions observed with this detector were 0.67 keV at 29.78 keV and 0.60 keV at 33.6 keV. Of course, efficiency will be a function of the sample thickness but this relationship is not as prevalent with $^{131\text{m}}\text{Xe}$ as it is with ^{133}Xe . The total efficiency for the K shell x rays was found to be 4.73% with 0.11 cc of $^{131\text{m}}\text{Xe}$ in the sample chamber. Although

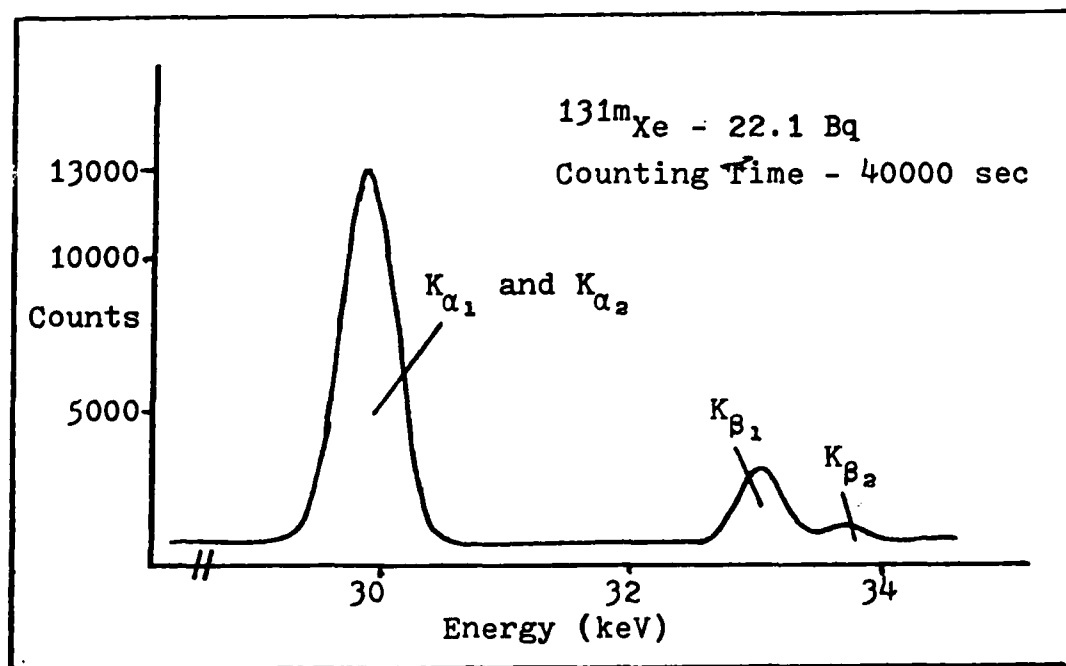


Figure 15. Xenon-131m X-ray Energy Spectrum

this does not approach the theoretical efficiency of 14.9%, it is significantly better than Hunt's value of 1.3%. The principal reason for this improvement is the increase in the geometry factor due to the system modifications previously discussed.

Xenon-133 Energy Spectra

Figure 16 shows an energy spectrum obtained with the electron detector with ^{133}Xe as the radioactive source. The characteristic cesium x rays and the xenon x rays due to carrier gas x-ray fluorescence are observed under a single photopeak at the lower end of the energy spectrum. Other than the beta spectrum associated with ^{133}Xe , the only other radiation which can be identified is the 81 keV gamma peak. The inter-

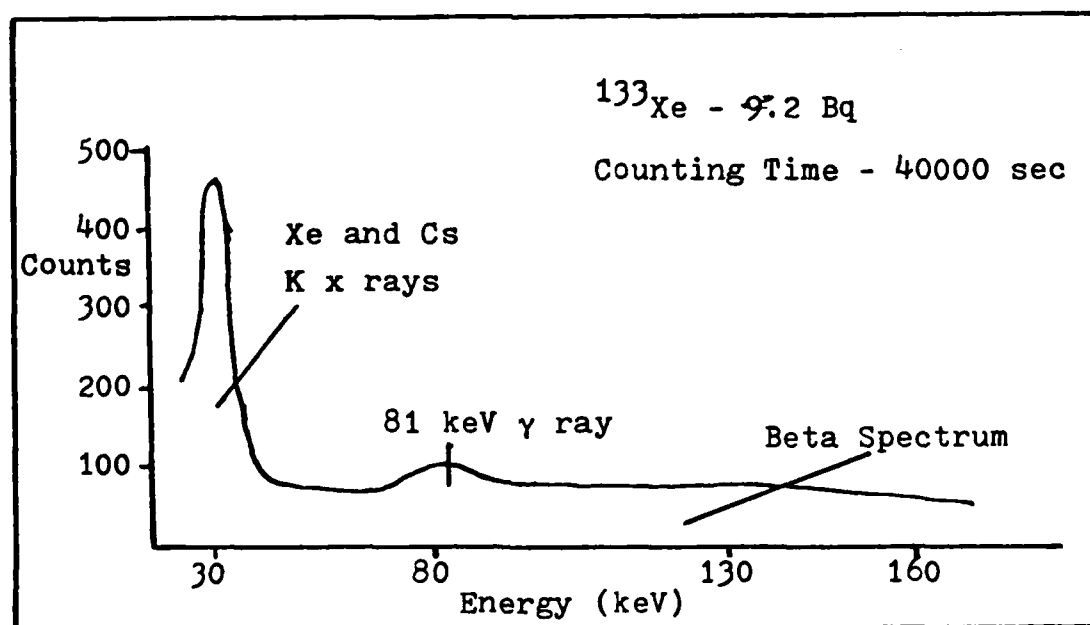


Figure 16. Xenon-133 Electron Energy Spectrum

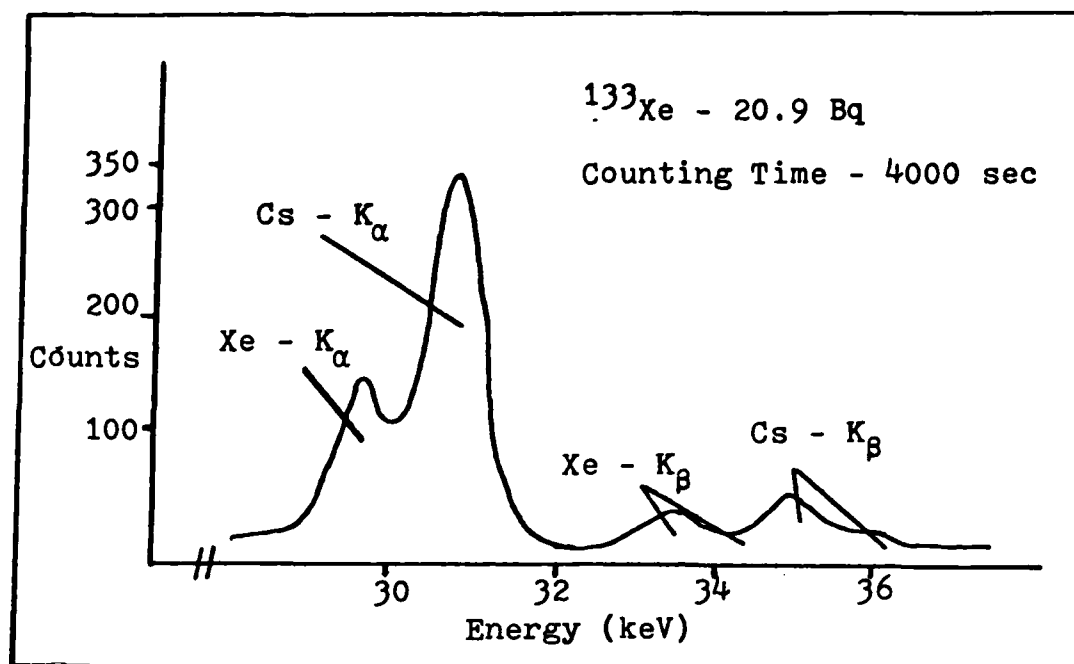


Figure 17. Xenon-133 X-ray Energy Spectrum

nal conversion electrons at 45 and 75 keV are not resolved.

The energy spectrum which was generated by the x-ray detector with ^{133}Xe as the radioactive source is shown in Figure 17. The most interesting aspects of this spectrum are the K_α and K_β xenon x-ray peaks in addition to the cesium x-ray peaks which one would expect to see with the decay of ^{133}Xe . As previously discussed, these peaks are a result of xenon carrier gas x-ray fluorescence and can be quantified. The resolution for the cesium K_α x-ray peak is similar to that observed with the xenon K_α peak (0.68 keV) and the total efficiency of the cesium K shell x rays was calculated to be 5.18%. In addition to the K shell x rays, a gamma-ray photopeak can be observed at 81 keV (not shown in Figure 17). Its resolution was calculated to be 0.77 keV and the total efficiency was 0.452%.

Combined Spectrum

Figure 18 represents an x-ray energy spectrum of a combination of ^{133}Xe and $^{131\text{m}}\text{Xe}$. The electron energy spectrum was similar to that of Figure 16 and the internal conversion electrons of $^{131\text{m}}\text{Xe}$ could not be identified. As far as the x-ray energy spectrum is concerned, the characteristic x-ray peaks of both cesium (decay of ^{133}Xe) and xenon (carrier gas fluorescence and the decay of $^{131\text{m}}\text{Xe}$) can be easily identified.

The procedure for determining the amount of $^{131\text{m}}\text{Xe}$ in the presence of ^{133}Xe involves three simple steps. But first, three very important values must be known in order to accomplish this task: 1) Total efficiency for the cesium x rays,

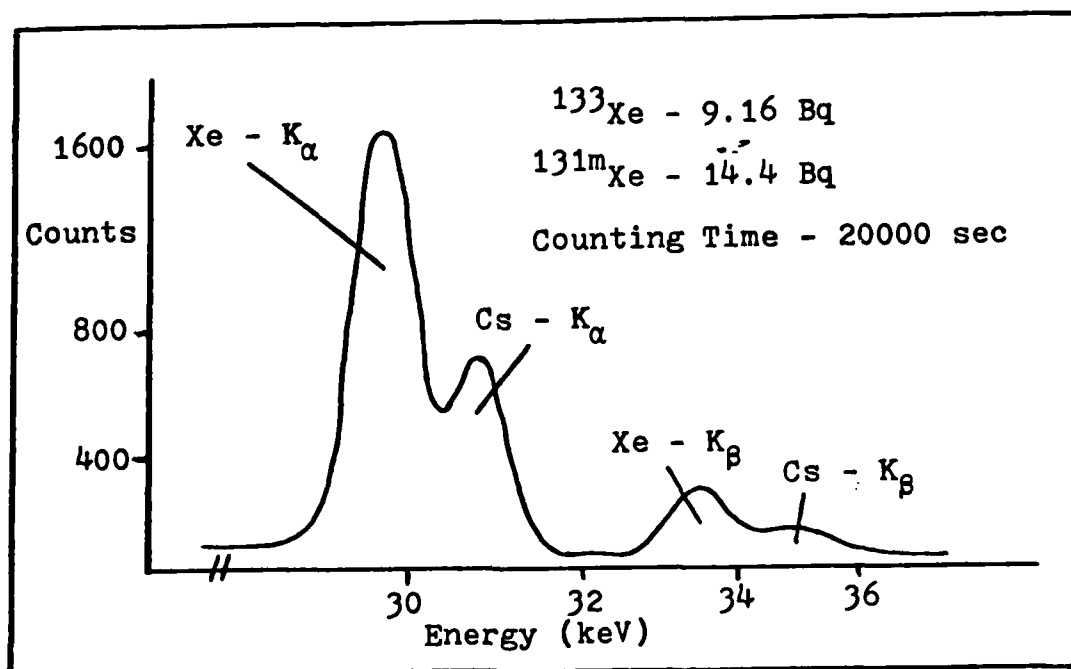


Figure 18. Combined X-ray Energy Spectrum of Both Xenon-133 and Xenon-131m

2) Total efficiency for the xenon x rays and, 3) The carrier gas x-ray fluorescence factor. First the activity of the ^{133}Xe sample is calculated using the number of counts under the cesium x-ray peaks and the total efficiency of the x-ray detector for cesium x rays. Second, the number of background counts would be determined and these calculated values would be subtracted from the total number of counts observed by the x-ray detector. The remainder is the number of xenon x rays from both the carrier gas fluorescence and the decay of $^{131\text{m}}\text{Xe}$. The number of xenon carrier gas fluorescence x rays can be calculated using the results previously discussed by applying the relationship of 0.01158 fluorescence x rays per second per 2.77×10^{-4} cm of sample thickness for 23 Bq of activity. This number is subtracted from the total number of counts observed. The resultant number is the quantity of xenon x rays from the decay of $^{131\text{m}}\text{Xe}$ and the activity of the $^{131\text{m}}\text{Xe}$ sample can be determined by simply knowing the total efficiency for xenon x rays. Using this procedure and the data from Figure 18, the activity of $^{131\text{m}}\text{Xe}$ was calculated to be 14.86 ± 0.38 Bq where the actual activity was 14.38 Bq. In this manner, the activity of $^{131\text{m}}\text{Xe}$ in the presence of ^{133}Xe can be determined.

VII. Conclusions and Recommendations

Conclusions

On the basis of the results presented in the preceding chapter, the following conclusions can be drawn concerning the characteristics of the radiation detection system under study:

1. The radioactive sample can now be deposited in the sample chamber in a predictable and reproducible manner.
2. The effect of self-absorption can be quantified and the experimental results agree very well with theory.
3. The effects of carrier gas fluorescence can also be experimentally quantified.
4. It is possible to experimentally determine the activity of ^{131m}Xe in the presence of ^{133}Xe using the three step procedure discussed in the previous chapter.

Recommendations

Based on observations made during this project the following recommendations are proposed for further study:

1. A calibration sample of ^{133}Xe should be obtained from the National Bureau of Standards and be used to determine the total efficiencies for the 81 keV

gamma ray and the cesium x rays of ^{133}Xe . These values are critical in the procedure to measure the activity $^{131\text{m}}\text{Xe}$ in the presence of ^{133}Xe .

2. Sample deposition area as a function of the amount of current applied to the the resistive heating wire should be investigated. Although the time it takes the sample to settle increases as less current is applied to the sample chamber, the deposition area should increase, the sample thickness decrease and thus the effects of self-absorption and carrier gas fluorescence should be minimized. This could be accomplished by repeating the procedure which was used in this study for the quantification of self-absorption and varying the amount of heat applied.
3. Examine the effects of sample size on the time required for the sample to complete its settling process. The results in this study were obtained using a constant sample size and varying the heat applied to the resistive heating wire.
4. The capabilities of this system for determining a very small amount of $^{131\text{m}}\text{Xe}$ in the presence of ^{133}Xe should be investigated. The results discussed previously were obtained with a ^{133}Xe to $^{131\text{m}}\text{Xe}$ activity ratio of 0.6367.

Bibliography

1. Bleuler, Ernest and G. J. Goldsmith. Experimental Nucleonics. New York: Rinehart & Company, Inc., 1956.
2. Chitwood, R. B. "Production of Noble Gases by Nuclear Fission," page 76 in Proceedings of the Noble Gas Symposium, ERDA CONF-730915, Stanley, R. E. and Moghissi, A. A., Editors, 1974.
3. Clark, George L. and Gessner G. Hawley, Editors, The Encyclopedia of Chemistry. New York: Van Nostrand Reinhold Company, 1966.
4. Cook, Gerald A., Editor. Argon, Helium, and the Rare Gases. New York: Interscience Publishers, 1961.
5. Hampel, Clifford A., Editor. The Encyclopedia of the Chemical Elements. New York: Reinhold Book Corporation, 1968.
6. Horrocks, D. L. "Measurement of Radioactive Noble Gases by Liquid Scintillation Techniques," page 201 in Proceedings of the Noble Gas Symposium, ERDA CONF-730915, Stanley, R. E. and Moshissi, A. A., Editors, 1974.
7. Horrocks, D. L. and M. H. Studier. "Determination of Radioactive Noble Gases with a Liquid Scintillator," Analytical Chemistry, 36:2077-2079 (October 1964).
8. Hunt, K. K. Analysis of a Semiconductor Detection System for Measuring Radioactive Noble Gases. Unpublished thesis. Wright-Patterson Air Force Base, Ohio: Air Force Institute of Technology, December 1976.
9. John, George. Professor, Department of Physics, Air Force Institute of Technology, Wright-Patterson Air Force Base, Ohio. Personal Interview. 9 December 1981.
10. Knoll, G. F. Radiation Detection and Measurement. New York: John Wiley & Sons, 1979.
11. Kocher, D. C. Radioactive Decay Data Tables, Technical Information Center, U. S. Department of Energy, 1981.
12. Lederer, C. M., et al. Table of Isotopes (Seventh Edition). New York: John Wiley & Sons, 1978.
13. McMaster, W. H., et al. UCRL 50174, Section II, Revision 1, Lawrence Radiation Laboratory, May, 1969.

14. Meek, M. E. and B. F. Rider. "Compilation of Fission Product Yields," Vallecitos Nuclear Center, ORNL-TM-3515, August, 1971.
15. National Council on Radiation Protection and Measurements. A Handbook of Radioactivity Measurements Procedures. 7910 Woodmont Avenue, Washington, D. C., November 1, 1978.
16. Nelms, A. T. Energy Loss and Range of Electrons and Positrons. NBS Circular 577. Washington, D. C.: USGPO, 1956.
17. Price, W. J. Nuclear Radiation Detection (Second Edition). New York: McGraw-Hill Book Company, 1964.
18. Rowe, C. R. Quantitative Analysis of Radioactive Noble Gases with a Si(Li) Detector. Unpublished thesis. Wright-Patterson Air Force Base, Ohio: Air Force Institute of Technology, March 1974.
19. Storm, E, et al. Gamma Ray Absorption Coefficients for Elements 1 to 100. LA-2237.
20. Walker, F. W. and G. J. Kirovac. "Chart of the Nuclides," Knolls Atomic Power Laboratory, Schenectady, New York, 1977.
21. Woldseth, R. All You Ever Wanted to Know About X-ray Energy Spectroscopy. Burlingame, CA: Kevex Corporation, 1973.

Appendix

Xenon-133 X-ray Energy Spectra Showing the Effects of Carrier Gas Fluorescence

The effects of carrier gas x-ray fluorescence on the x-ray energy spectra of Xenon-133 can be seen in Figures 19-23. Figure 19 shows the x-ray energy spectrum generated by Xenon-133 with a sample thickness of 0.02766 cm and an activity of 23 Bq. For the next four figures, the activity of the sample was held constant while the sample thickness was increased in four increments of 5.532×10^{-3} cm apiece. One can see how the xenon K_{α} x-ray peak grows linearly with each increase in sample thickness while the cesium K_{α} peak remains constant because of the constant activity of the sample. The increases in the xenon x-ray peaks is a result of carrier gas x-ray fluorescence.

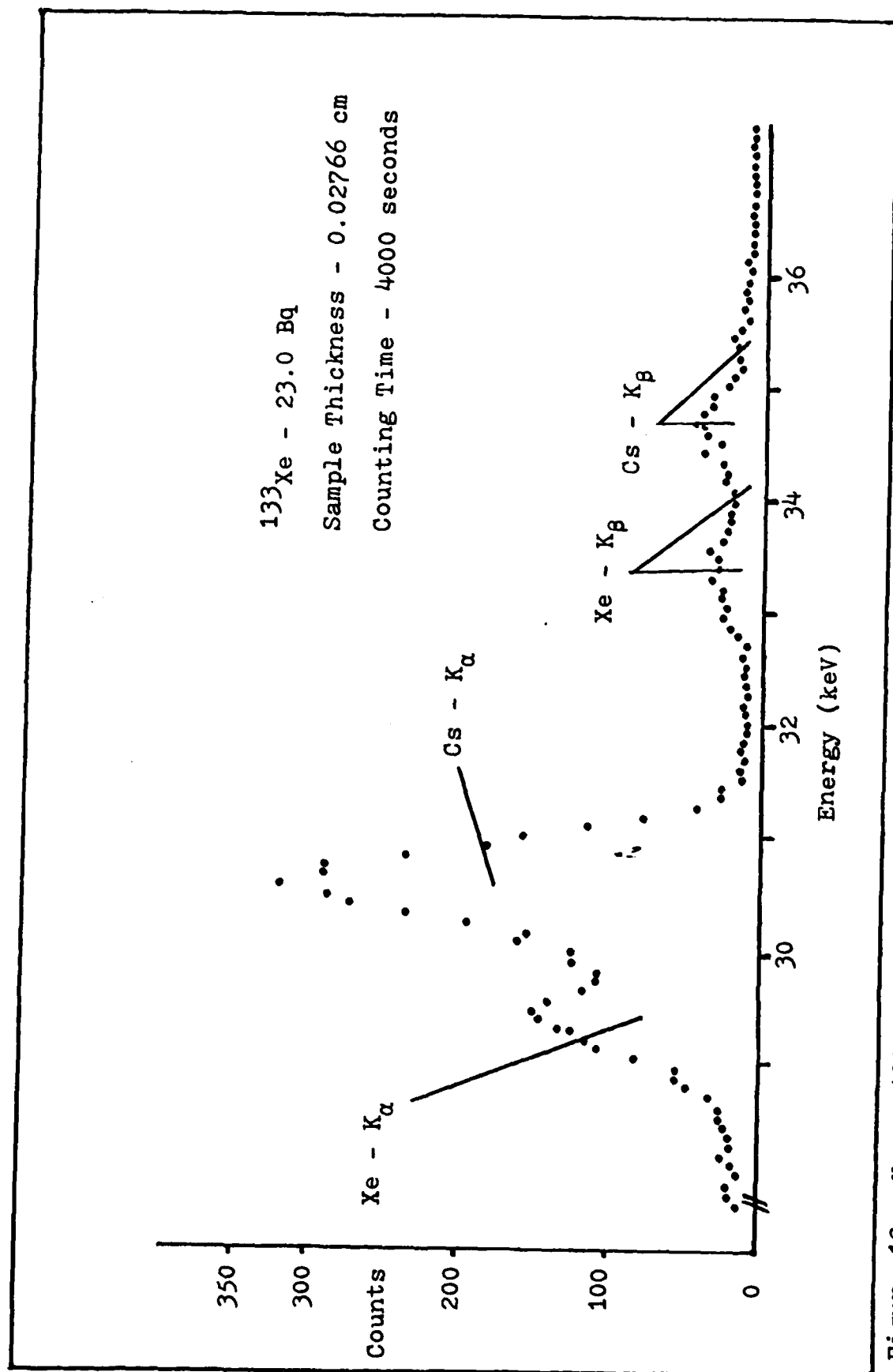


Figure 19. Xenon-133 X-ray Energy Spectrum - Sample Thickness = 0.02766 cm

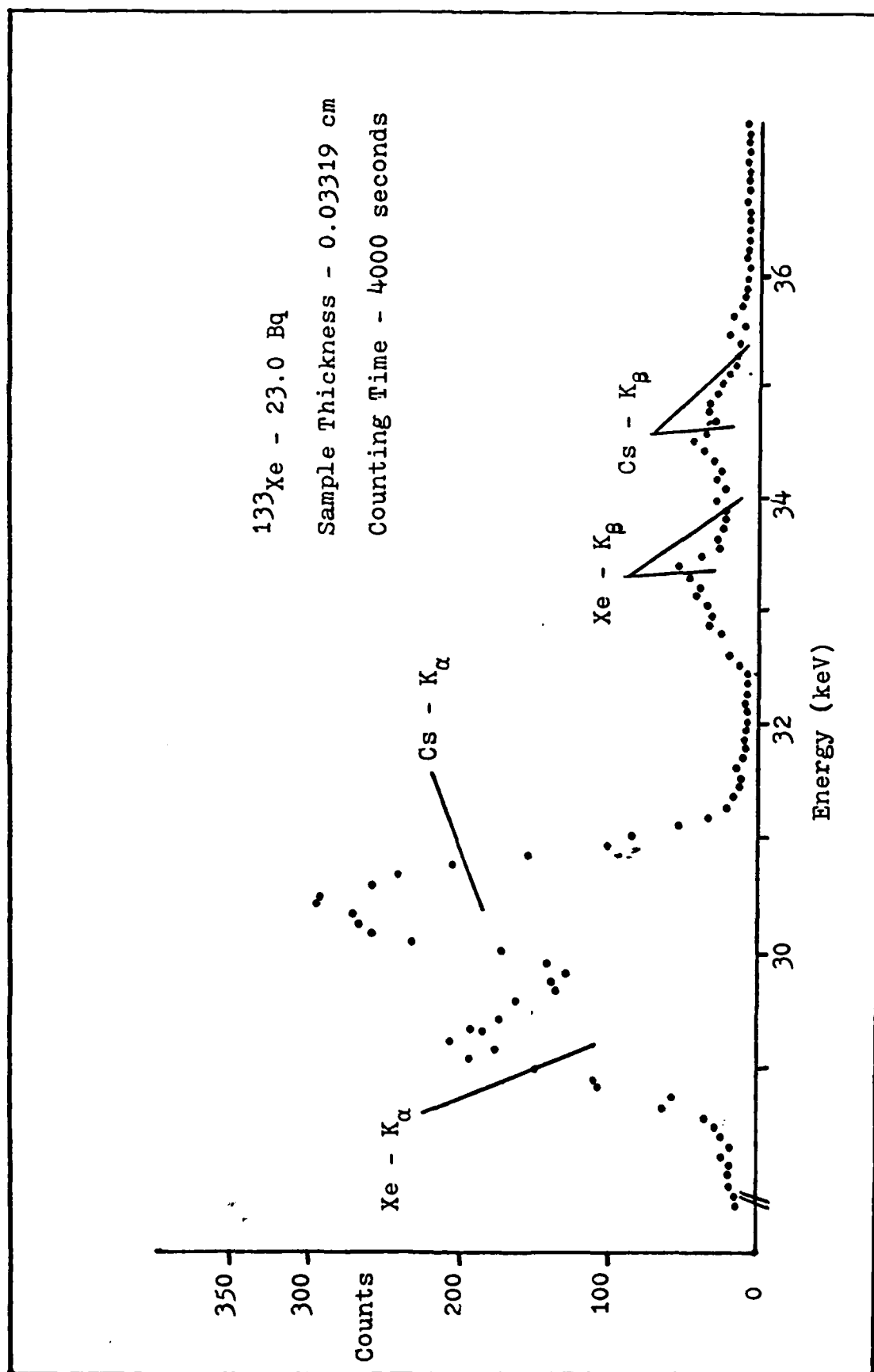


Figure 20. Xenon-133 X-ray Energy Spectrum - Sample Thickness = 0.03319 cm

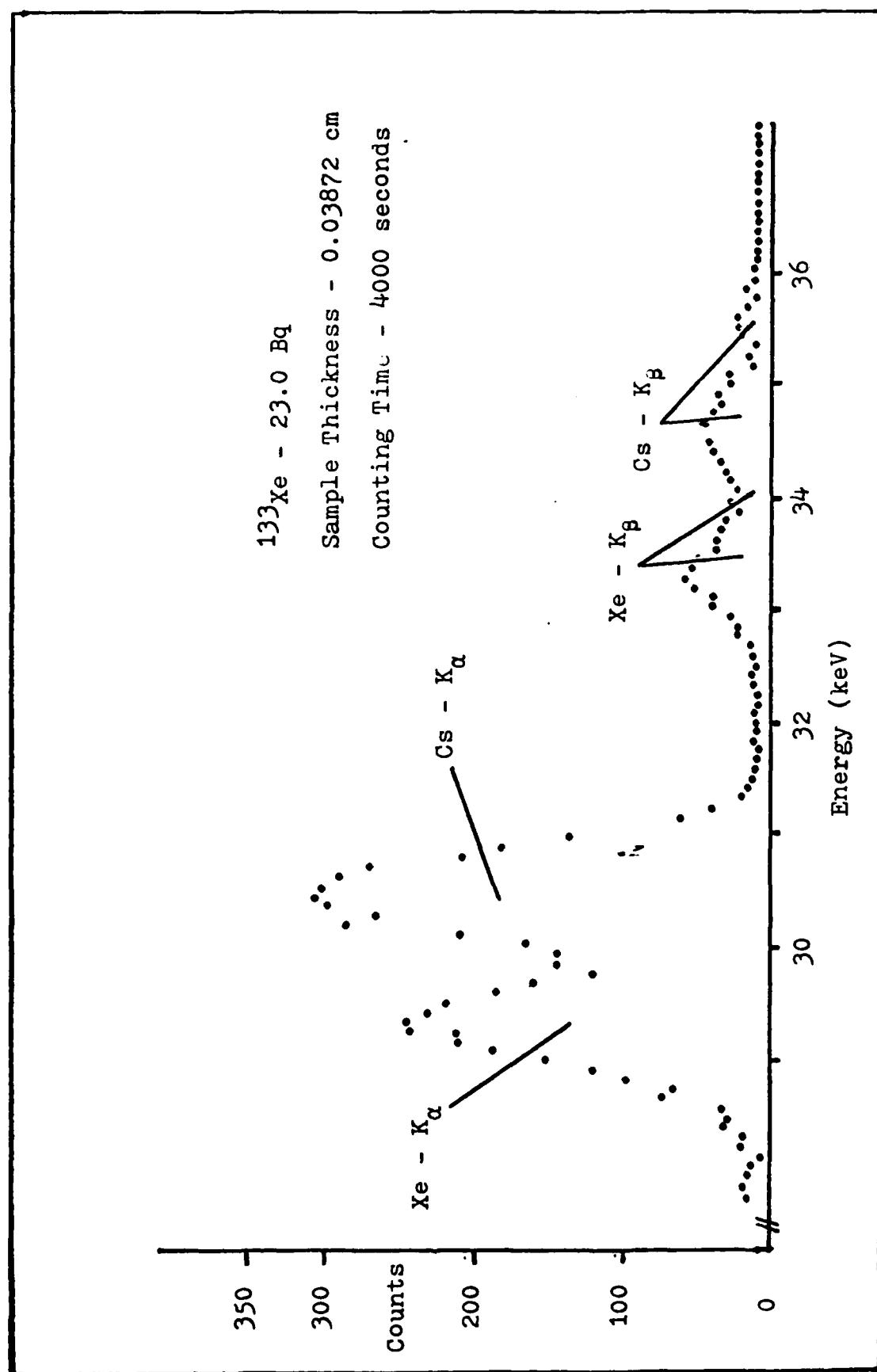


Figure 21. Xenon-133 X-ray Energy Spectrum - Sample Thickness = 0.03872 cm

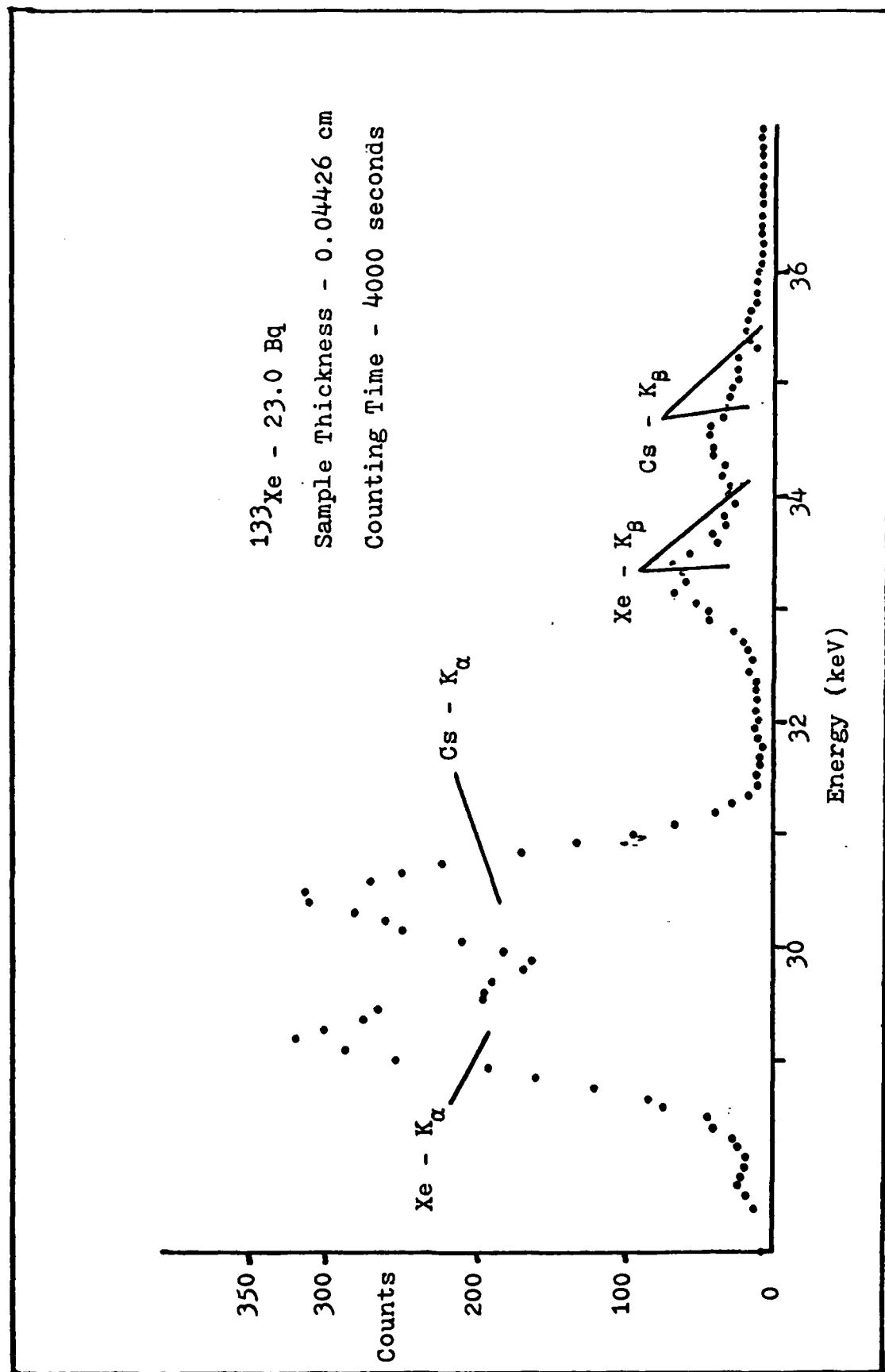


Figure 22. Xenon-133 X-ray Energy Spectrum - Sample Thickness = 0.04426 cm

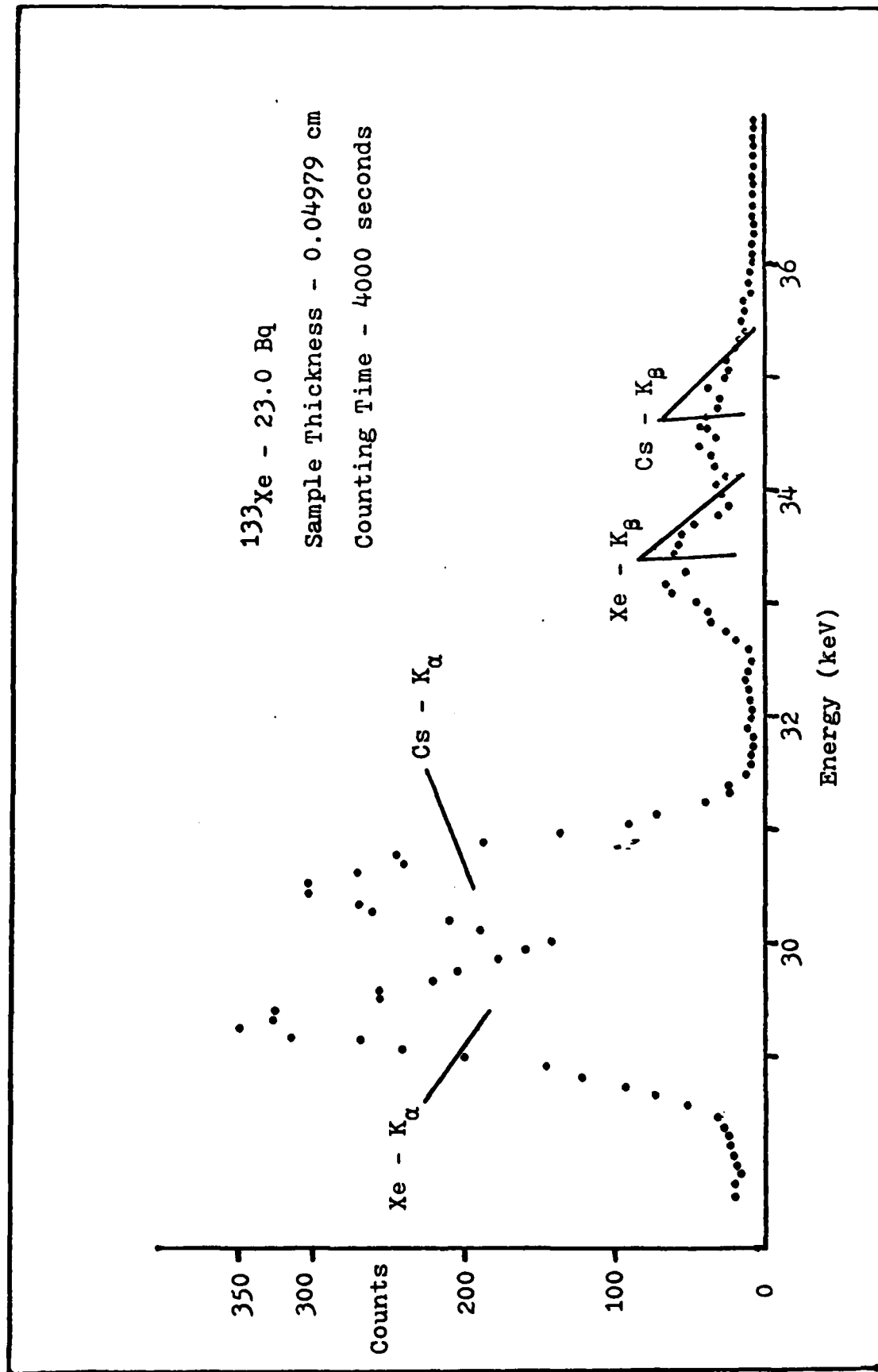


Figure 23. Xenon-133 X-ray Energy Spectrum - Sample Thickness = 0.04979 cm

Vita

Wayne Linwood Andrews, Jr. was born on 4 May 1952 in Salem, Massachusetts. He graduated from Salem High School in 1970 and attended the United States Coast Guard Academy. In 1973 he enrolled in the Engineering College of the University of Lowell, Lowell, Massachusetts, from which he received the degree of Bachelor of Science in Nuclear Engineering in May 1975. Upon graduation he received his commission in the United States Air Force and entered the Air Force on active duty in February 1976. He served as a Missile Combat Crew Commander - Instructor with the 321st Strategic Missile Wing at Grand Forks AFB, North Dakota. In May 1979 he received the degree of Master in Business Administration from the University of North Dakota and in August, 1980 he entered the School of Engineering, Air Force Institute of Technology.

Permanent address: 9 Arrow Drive

Salem, New Hampshire 03079

UNCLASSIFIED

SECURITY CLASSIFICATION OF THIS PAGE (When Data Entered)

REPORT DOCUMENTATION PAGE		READ INSTRUCTIONS BEFORE COMPLETING FORM
1. REPORT NUMBER AFIT/GNE/PH/82M-1	2. GOVT ACCESSION NO. AD-A124796	3. RECIPIENT'S CATALOG NUMBER
4. TITLE (and Subtitle) EVALUATION OF A DETECTION SYSTEM EMPLOY- ING TWO SILICON SEMICONDUCTORS FOR THE ANALYSIS OF RADIOACTIVE NOBLE GASES		5. TYPE OF REPORT & PERIOD COVERED MS Thesis
7. AUTHOR(s) Wayne L. Andrews, Jr Capt USAF		6. PERFORMING ORG. REPORT NUMBER
9. PERFORMING ORGANIZATION NAME AND ADDRESS Air Force Institute of Technology (AFIT-EN) Wright-Patterson AFB, Ohio 45433		8. CONTRACT OR GRANT NUMBER(s)
11. CONTROLLING OFFICE NAME AND ADDRESS		10. PROGRAM ELEMENT, PROJECT, TASK AREA & WORK UNIT NUMBERS
14. MONITORING AGENCY NAME & ADDRESS (if different from Controlling Office)		12. REPORT DATE March 1982
		13. NUMBER OF PAGES 72
		15. SECURITY CLASS. (of this report) UNCLASSIFIED
		15a. DECLASSIFICATION/DOWNGRADING SCHEDULE
16. DISTRIBUTION STATEMENT (of this Report) Approved for public release; distribution unlimited		
17. DISTRIBUTION STATEMENT (of the abstract entered in Block 20, if different from Report)		
18. SUPPLEMENTARY NOTES <div style="text-align: right;"> <p>Approved for public release; LAW, AFR 100-17. LYNN E. WOLAVER Dean for Research and Professional Development Air Force Institute of Technology (AFIT) Wright-Patterson AFB OH 45433</p> </div>		
19. KEY WORDS (Continue on reverse side if necessary and identify by block number) Xenon Semiconductor Detectors Radioactive Noble Gases Detection and Measurement Lithium-Drifted Silicon (Si(Li))		
20. ABSTRACT (Continue on reverse side if necessary and identify by block number) This report presents a study of the characteristics of a radiation detection system for the analysis of radioactive noble gases. The sample gas is condensed in a chamber between two planar lithium-drifted silicon semiconductor detectors. The analysis was limited to two radioisotopes of xenon, ^{131m}Xe and ^{133}Xe , which are produced in nuclear fission. X-ray spectroscopy was used in an attempt to quantify ^{131m}Xe in the presence of ^{133}Xe . In previ-		

DD FORM 1473

JAN 73

EDITION OF 1 NOV 65 IS OBSOLETE

UNCLASSIFIED

SECURITY CLASSIFICATION OF THIS PAGE (When Data Entered)

19 JAN 1983

UNCLASSIFIED

SECURITY CLASSIFICATION OF THIS PAGE(When Data Entered)

ous research using this system, the sample gas deposited itself in the sample chamber in an uneven and unpredictable manner. Modifications were made to the sample chamber and the gas now deposits itself predictably and reproducibly. Also, the effects of self-absorption and carrier gas x-ray fluorescence were analyzed and quantified. Finally, it was found that the system could quantify ^{131}mXe in the presence of ^{133}Xe using a simple three step procedure. Recommendations were made for further study with this system.

UNCLASSIFIED

SECURITY CLASSIFICATION OF THIS PAGE(When Data Entered)

END